Carbon Letters (2022) 32:1–38
https://doi.org/10.1007/s42823-021-00272-z

Online ISSN 2233-4998
Print ISSN 1976-4251

REVIEW

Graphene oxide synthesis using a top–down approach and discrete characterization techniques: a holistic review

Abdullah Anwar[1,2] · **Ta-Peng Chang**[1] · **Chun-Tao Chen**[1]

Received: 5 June 2021 / Revised: 27 July 2021 / Accepted: 1 August 2021 / Published online: 12 August 2021

Abstract

The remarkable electrical, thermal, mechanical, and optical properties of graphene and its derivative grapheme oxide have recently gained great importance, along with the large surface area and single-atoms thickness. In this respect, several techniques of synthesis such as chemical exfoliation, mechanical exfoliation, or chemical synthesis have been discovered. However, the development of graphene with fewer defects and on a large scale poses major challenges; therefore, it is increasingly necessary to produce it in large proportions with high quality. This paper reviews the top-down synthesis approach of graphene and its well-known derivative graphene oxide. Furthermore, characterization of graphene oxide nanomaterial is a critical component of the analysis. The characterization techniques employed to determine the quality, defects intensity, number of layers, and structures for graphene oxide nanomaterial at the atomic scale. This article focuses on the different involved characterization methodology for graphene oxide with their percentage utilization for the past 11 years. Additionally, reviewing all of the characterization literature for the last 11 years would be a difficult task. Therefore, the aim is to outline the existing state of graphene oxide by different characterization techniques and provide a comparative analysis based on their percentage utilization.

Keywords Graphene · Graphene oxide · Synthesis · Fabrication · Characterization

1 Introduction

Recent advancement in the field of nanotechnology has initiated the development of innovative nanoscale fibers which led to the origin of multifunctional materials [1] with advanced sensing [2], high-performance nanocomposite [3–5]. Since the end of 1974, the term 'nanotechnology' has been used by Dr. Norio Taniguchi in his speech titled "Basic concept of Nanotechnology". Nanotechnology is associated with the utilization of extremely smaller constituents in order of lesser than 100 nm [6, 7]. Precisely, nanotechnology is defined as the application of very small-sized particles of materials for the formation of large-sized novel materials [8, 9]. Undeniably, the nanomaterials deal with the innovative characteristics of the material at nanoscales and unveiling their significant properties [10, 11]. As per the report of the Columbia Engineering team, in Science Daily (2013), stated that in its perfect crystalline form, graphene is the strongest material ever measured [12]. The Graphene era of nanotechnology research is growing in a very hotfoot manner, as a noteworthy potential to widespread in multiple domains. This development is being made possible with the funding of RM 156 million for the 10th Malaysia Plan (RMK10), and by the adoption, in the 11th Malaysia Plan (RMK11) of the National Graphene Action Plan (NGAP) 2020, defined as the "Strategic and Calculated Venture on Graphene" [13]. In addition to the above, *The European Union* has earmarked one billion Euros on the study the Graphene by *Horizon 2020*, a program for funding research and innovation as well as financial instrument for the development of "Innovation Union", one of the "Flagship Initiatives" of Europe 2020 [14]. In year 2020, the estimated market value of graphene was around €100 million that is projected to increase in range of €150–500 million in 2025 [15]. Altogether, graphene is one of the strongest and most promising nanomaterials presenting the novelty in its behavior.

✉ Abdullah Anwar
a.anwar14330@gmail.com

[1] Department of Civil and Construction Engineering, National Taiwan University of Science and Technology, 106 Taipei, Taiwan, R.O.C.

[2] Department of Civil Engineering, Integral University, Lucknow, Uttar Pradesh 226026, India

Graphene is referred to as the monoatomic graphite layer [16, 17]. Graphene is a 2D planar layer of a single hybridized atomic dense carbon allotropic, which is kept together by the strong van der Waals effects, which building block with the bundled carbon atoms in the shape of a honeycomb structure (thickness: 0.335 nm) [18]. It is considered as the backbone for all graphitic materials irrespective of their dimensionalities and can be enfolded in zero-dimensional (fullerenes), one-dimensional (nanotubes), or piled in three-dimensional (graphite) (Fig. 1) [19, 20]. Graphene above 5 and up to 30 layers are generally referred to as multilayer/thicker sheets [6]. The distance of carbon to carbon bond is 0.142 nm with a layer height of approximately 0.335 nm creating a hexagonal layer that allows it to diffuse effectively (Fig. 2) [21]. In 2002, *ab-initio* calculations showed that a graphene sheet is thermodynamically unstable if its size is less than about 20 nm and it becomes the most stable fullerene (within graphite) only for molecules larger 24,000 atoms [22–24]. The hierarchy for the most stable carbon phase based on carbon atoms at nanoscale is shown in Fig. 3 [23]. Graphene was recognized since the first graphite oxide paper mentioned by the Kohlschutter in 1918 [25] and its structure was determined by Bernal in 1924 from single-crystal diffraction method [26]. However, it was known in 2004 by Andre Geim and Konstantin Novoselov after their pioneering research work (awarded Nobel Prize in Physics, 2010). Graphene films have been effectively developed by a mechanical exfoliation process (repeated peeling) [21]. Goyenola et al [27] studied the carbon-based thin film structure using a synthetic growth concept (SGC) based on density functional theory (DFT). It is an efficient technique in analyzing and modeling the properties of carbon-based nano-structured materials such as graphene. The bonding distance among the carbon atoms (C–C) distributed in the formation of its structural element identifies the degree of disorder, density, and other structural properties. Due to its novel 2D microstructure, graphene possesses extraordinary physiochemical properties to constitute of adjacent carbon

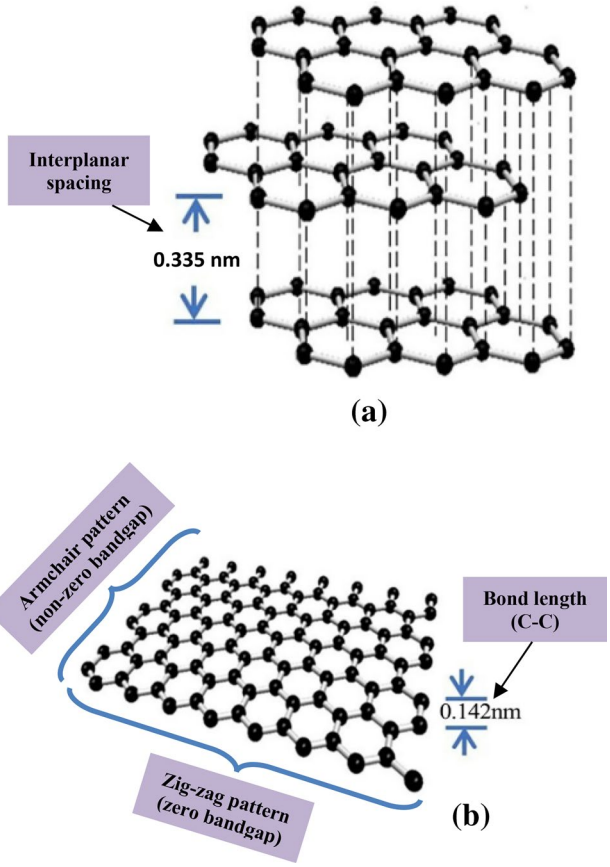

Fig. 2 Graphene hexagonal layered structure: **a** Interlayer thickness of 0.33 nm; **b** carbon to carbon bond length of 0.142 nm [21]

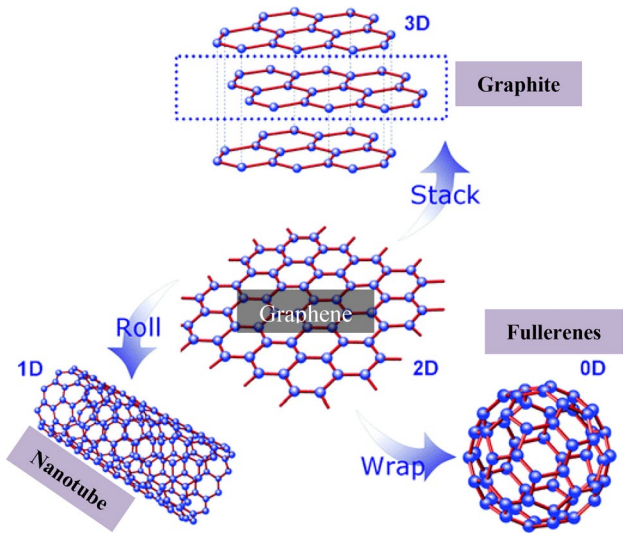

Fig. 1 Graphene—Backbone of all graphitic carbon allotropes. Adapted with permission from [20]

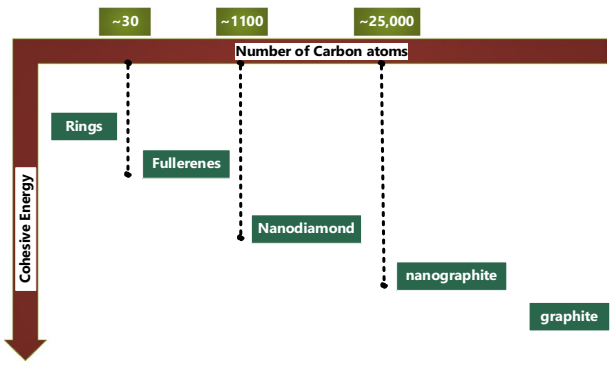

Fig. 3 Hierarchy for most stable carbon phase based on size of carbon structure [23]

atoms bonded by single and double covalent bonds arranged in an alternative manner.

Owing to this astounding phenomenon of microstructure, graphene has exceptional properties, with broad surface area (2630 m^2 g^{-1}), larger intrinsic mobility (200,000 cm^2 V^{-1} s^{-1}) [28], strong Young modulus (~ 1.0 TPa), and heat conductivity (~ 5000 Wm^{-1} K^{-1}) [29]. Additionally, it possesses better optical transmission (~ 97.7%) [12], greater electrical conductivity, and the ability to resist a current density of 108 A/cm^2 [30]. Graphene is also known as a null-band semiconductor so that a specific physical and chemical process may change its band gap [29]. Graphene can be synthesized into various forms depending on its usage and applications in research and industrial sectors. This includes fabrication of graphene oxide, graphene nanosheets, reduced GO (rGO), multilayer grapheme (MLG), graphene nanoribbon, few layers grapheme (FLG), bilayer and tri-layer graphene, graphene microsheet, graphene quantum dots (GQD), graphene nanoplates (GNPs), and graphene nanoflakes (Fig. 4) [31]. Graphene oxide (GO) is considered as one of the most prevailing highly oxidized graphene derivative based on its microstructural properties such as the presence of abundant oxygen functional groups and enormous surface area constructing it highly reactive in nature (especially in field of civil engineering) [32–36]. GO is a kind of two-dimensional (2D) nanomaterial that possesses not only the property of 1-D nanomaterial but also includes sp^2-bonded carbon atoms that express graphene with outstanding mechanical properties [37]. Extensive structural classes of oxygen functional groups include hydroxyl (–OH), epoxide (–O–), carboxylic (–COOH), and carbonyl (–COO) exhibits on GO surface (Fig. 5) which

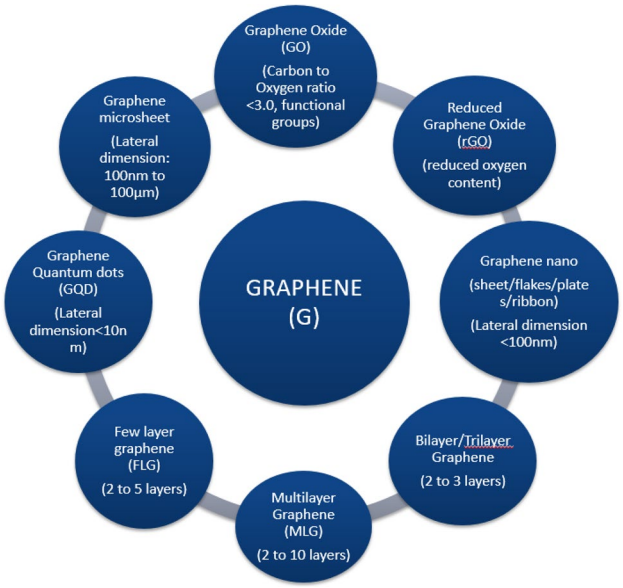

Fig. 4 Different forms of graphene

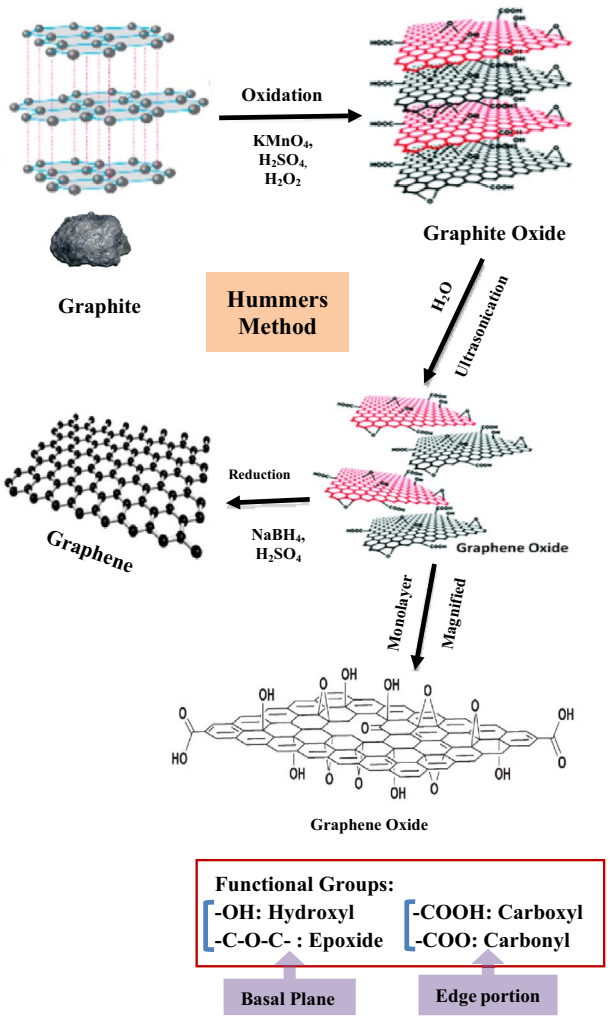

Fig. 5 Schematic representation of GO fabrication. Adapted with permission from [39, 40]

enhances its dispersion in water [16, 38]. Therefore, graphene has emerged as an exceptional futuristic nanomaterial of the twenty-first century, receiving concentration globally, due to its extraordinary transport, thermal, optical, and mechanical behavior (Fig. 6).

Graphene developed by micromechanical graphite cleavage was a simple, high quality, but time-intensive process and not possible for bulk production. Different alternative techniques for producing and synthesizing graphene include chemical vapor deposition (CVD), chemical exfoliation, mechanical exfoliation, epitaxial growth, graphite oxide reduction, CNT degradation, pyrolysis, grafting, and self-exfoliation have been reported recently [41, 42]. Graphite chemical oxidation is the most used GO synthesis method and introduces the oxygen-based functional groups among graphite layers [43]. GO can be generated with cheap graphite as the raw material by the cost-effective chemical process. The chemical process involves graphite-to-GO oxidation

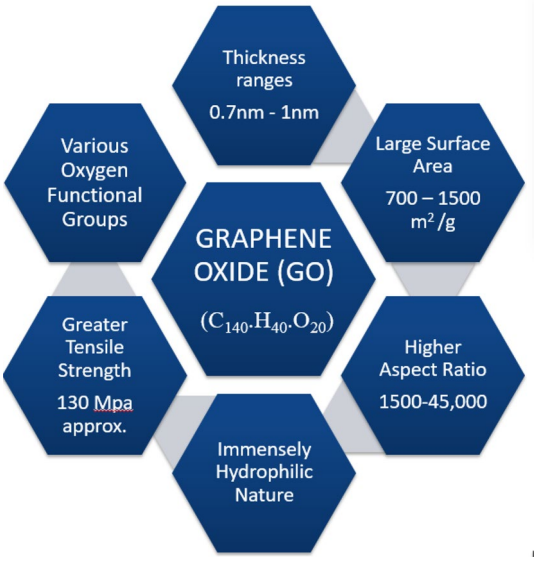

Fig. 6 Schematic representation of GO properties

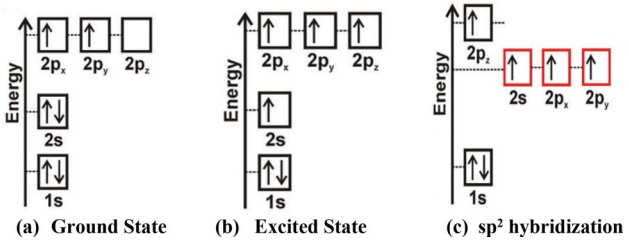

Fig. 7 Representation of valence electrons of the carbon atoms for sp^2 hybridization. Adapted with permission from [48]

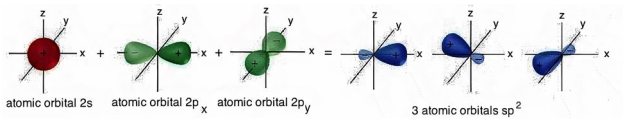

Fig. 8 Graphical representation sp^2 hybrid atomic orbitals [47]

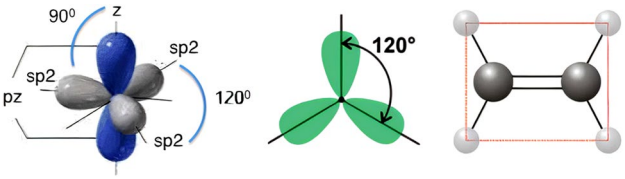

Fig. 9 Planar triangular structure for sp^2 hybridization. Adapted with permission from [47, 48]

with strong oxidizing agents [44]. The production of a large amount of powdered GO is both a benefit and convenient due to its cost-efficiency and a quality gain approach [45]. The method consists of graphite oxidation and exfoliation into single-layered or few-layered GO sheets. The common Hummer process usually involves many phases, a repetitive and long processing period, and temperature control for GO preparation, so the simpler Hummers process is commonly used for GO manufacturing [46]. GO characterization techniques include Fourier Transform Infrared Spectroscopy (FTIR), Energy Dispersive X-Ray Spectroscopy (EDX), Raman Spectroscopy, Field Emission Scanning Electron Microscopy (FE-SEM), Nuclear Magnetic Resonance (NMR) and many more. This article critically reviews the different methods involved in the top–down approach for the fabrication of GO. Moreover, this paper also discusses the recent techniques involved in the characterization of GO nanomaterial with its varying utilization percentage.

2 Graphene: sp^2-hybridization

In the structure of graphene, the carbon atoms are sp^2 hybridized and can be bonded ensuing the development of a 2D honeycomb structure [47]. A carbon atom has six protons and six electrons, two electrons occupy the "1s" atomic orbital and they are strongly bound. Two of the other four electrons (the valence electrons) are paired and occupy the "2s" atomic orbital. The remaining two unpaired electrons occupy different "2p" atomic orbitals; then the electron configuration of the carbon atom can be rewritten in the form of $1s^2 2s^2 2p_x 2p_y$ (Fig. 7) [48]. The "2s" and "2p" atomic orbitals of the carbon atom have very similar energies; therefore, the electrons belonging to them can move very easily, generating, in this way, the hybridization phenomenon. The 2s atomic orbital and the two atomic orbitals of 2p ($2p_x$ and $2p_y$) are mixed which results in the formation of three hybrid atomic orbitals called ***sp^2-atomic orbitals*** (Fig. 8) [47]. These atomic orbitals are iso-energetic, perfectly equivalent, oriented symmetrically in a plane, form angles of 120°, and give rise to the so-called *planar triangular structure* (Fig. 9) [48]. The fourth atomic orbital "$2p_z$" is not involved in the hybridization process and acts perpendicular to the plane on which sp^2 hybrid atomic orbitals were located [47].

When two sp^2 hybridized carbon atoms come close to each other, they form a strong σ-bond by overlapping the sp^2–sp^2 hybrid atomic orbitals. In addition, also the p atomic orbitals, not hybridized but still present in each carbon atom, come closer so that they overlap and form a π-bond as shown in Fig. 10 [47].

In sp^2-hybridization, each atom has three σ-bonds available on the x–y plane, which results in the formation of a honeycomb structure. The p_z atomic orbitals come together and form a π-bond, located above and below the x–y plane (Fig. 10) [47]. The stronger σ-bonds and weak π-bond forms the two-dimensional honeycomb lattices structure held

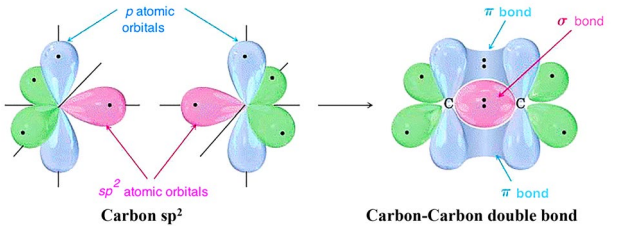

Fig. 10 Formation of σ-bonds and π-bond in an sp^2 hybridization [47]

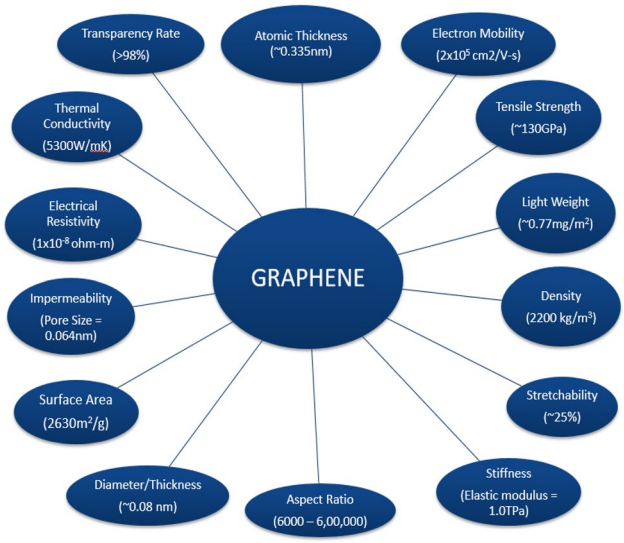

Fig. 11 Schematic representation of graphene properties

together with one on the other by weak interaction forces called "Van der Waals (vdw)" forces [47, 48]. The formation of these bonds by sp^2 atomic orbitals originates from the nanostructure of graphene.

3 Properties of graphene nanomaterial

Graphene is the building block for all graphitic materials. Based on literatures [49, 50], the properties of graphene presenting its enormous potential (Fig. 11) are as follows:

a. Atomic thickness: Graphene is the world's first man-made 2D material consisting of a single layer of carbon atoms arranged in a honeycomb structure. Its atomic thickness in about 0.335 nm. For better interpretation, thickness of one million graphene layers is equal to the thickness of the human hair [51, 52].
b. Electron mobility: It has the highest electron mobility among all electronic materials with theoretical limit of 200,000 cm^2/V-s. Its electron mobility is even 100 times faster than silicon material [53].
c. Strength: Graphene is one of the strongest known material and even harder than diamond. A defect free, graphene monolayer has strength of 130 GPa that is 100 times stronger than the strongest steel [49].
d. Toughness and stretchiness: It is tougher than steel and yet lighter than aluminum. Its stretchable properties are higher by up to 25% that may explore new dimensions in stretchable optoelectronics field [49, 54].
e. Stiffness: Defect free graphene yielded young modulus of about 1.0 TPa that is one of the highest value achieved by any material [49].
f. Weight and surface area: It is incredibly light weighing approx. 0.77 mg/m^2 and possess very high surface area of 2630m^2/g [28]. For better perspective, with less than 3 gm of graphene material an entire soccer field may be covered up [55].
g. Impermeability: It is the most thinnest impermeable material (geometric pore size—0.064 nm) that does not allow even the smallest atom helium (pore size—0.28 nm) to pass through it except water molecules [52].
h. Electrical resistivity: It is a superb conductor with least electrical resistivity (1×10^{-8} Ω-m) and greatly reduced energy losses. It has electrical resistivity is almost 35% less than copper [53].
i. Thermal conductivity: It possesses a very high thermal conductivity up to 5300 W/mK at room temperature. It conducts heat 2 times better than diamond and non-flammable in nature [56].
j. Transparency: It is an incredibly transparent and flexible material. Its optical transmission rate is around more than 98%, which is even higher than indium tin oxide (ITO) glass substrate (85%) [57].

4 Synthesis of graphene nanomaterial

The synthesis of graphene nanomaterial and its oxides involves two major approaches:

(a) *Top–down approach*: In this method, the larger structures are reduced to nanoscale size while maintaining their original properties without atomic-level control, i.e., miniaturization in the domain of electronics or deconstructed from larger structures into their smaller, composite parts (Fig. 12) [58, 59]. For example, making a wooden plank from a tree or fabrication of silicon wafers from silicon ingots. Moreover, the top-down approach is more advantageous in the synthesis of graphene nanomaterial as they can scale up to produce larger quantities than bottom-up approaches [60].

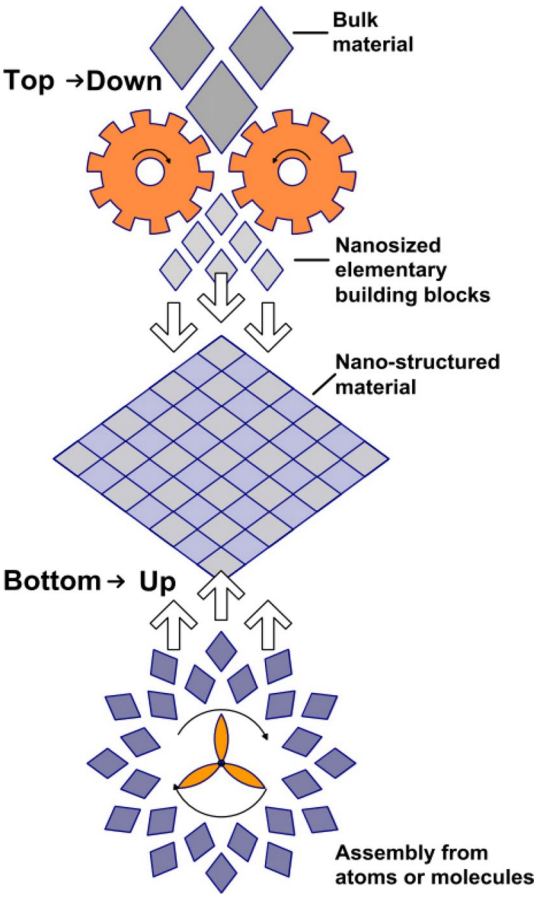

Fig. 12 Top–down and Bottom–Up approach for the synthesis of nanomaterial. Adapted with permission from [59]

(b) *Bottom–Up approach*: This technique was introduced by Drexler et al. [61]. In this method, the materials are engineered from atomic or molecular components through the process of assembly or self-assembly. This approach is also known as molecular nanotechnology or molecular manufacturing (Fig. 12) [58, 59]

The method by which graphene nanomaterial and its oxides are processed or extracted according to the necessary specifications and quality is known as a graphene synthesis. To date, several approaches to graphene synthesis and its derivatives have been established. Extensive investigations were undertaken about mechanical cleaving (exfoliation), chemical synthesis, chemical exfoliation, epitaxial growth, and thermal chemical vapor deposition methods [62, 63]. Other methods have been reported, including electrochemical exfoliation, microwave synthesis, and CNT unzipping [64, 65]. While AFM cantilever mechanical exfoliation was found to be able to generate few graphene sheets, the process limitations varied graphene thickness to about 10 nm comparable to 30 layer grapheme [66]. Specifically, large-scale graphene synthesis comprising of single-level graphene (SLG), bilayer graphene (BLG), and few-layer graphene (FLG) may be acquired using top–down and bottom–up techniques. Since most contemporary technologies rely on the "top–down" technique [58], therefore, this review article presents the different methods involved in a top–down process for the synthesis of graphene oxides due to its simplicity, efficient and widespread approach. Figures 13 and 14 presents the flowchart and graphical representation for the categorization of different fabrication techniques including both top–down and bottom–up approach with its essential features and applications [67].

5 Top–down process

Graphene sheets are formed in the top–down process by exfoliating or separating graphite or graphite derivatives such as GO.

5.1 Mechanical exfoliation

The first approach to extract graphene flakes on a surface is mechanical exfoliation [68]. It is possible employing different agents like scotch tape, electric field, and

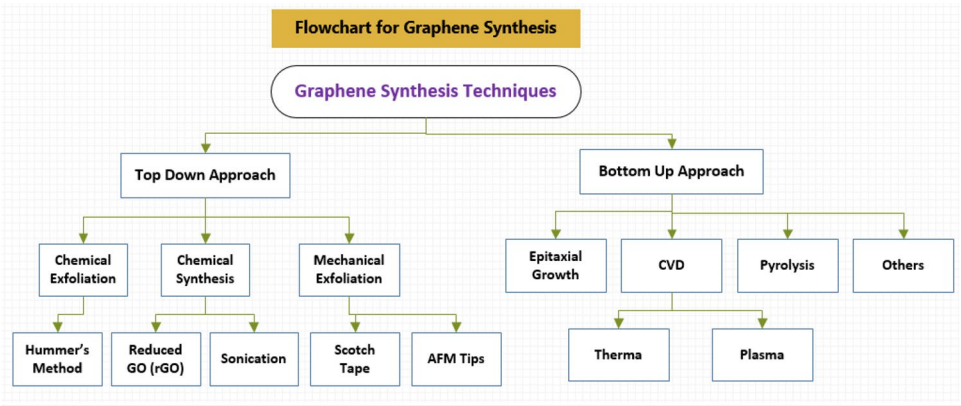

Fig. 13 Graphene synthesis process flowchart [67]

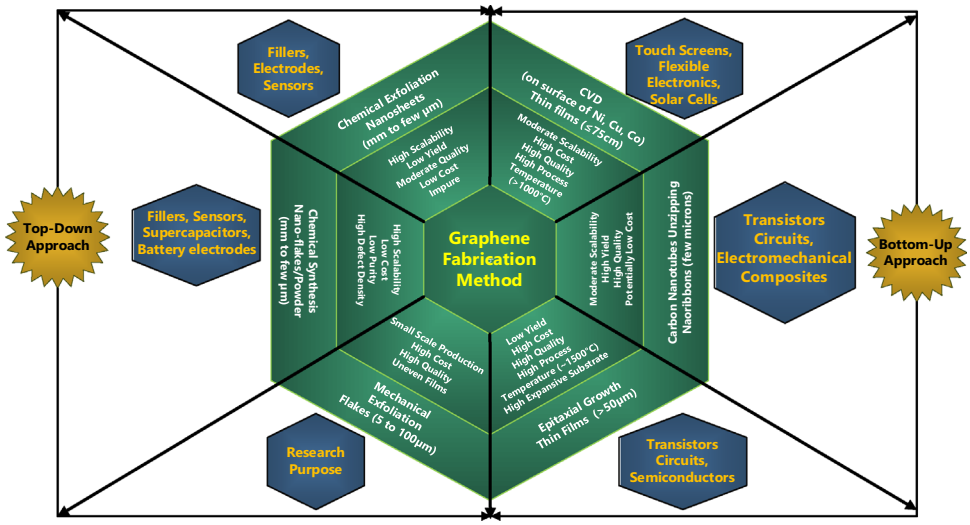

Fig. 14 Conventional methods used for graphene fabrication with essential features and applications [75]

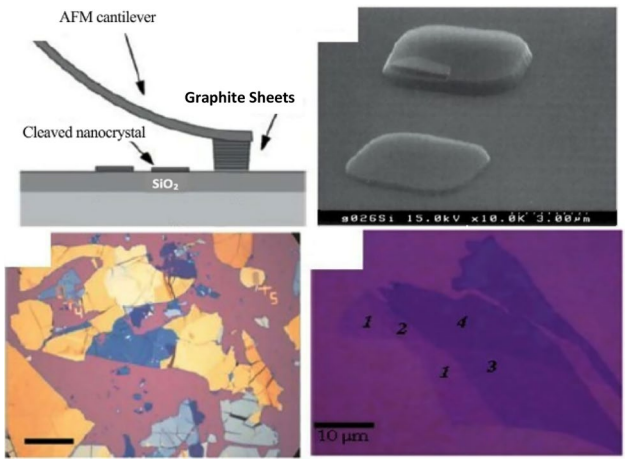

Fig. 15 **a** Mechanical exfoliation via AFM; **b** Exfoliated graphite surface using SEM analysis; **c** Mechanical exfoliation utilizing scotch tape; **d** SiO_2/Si substratum containing graphene layers of different thickness [73]

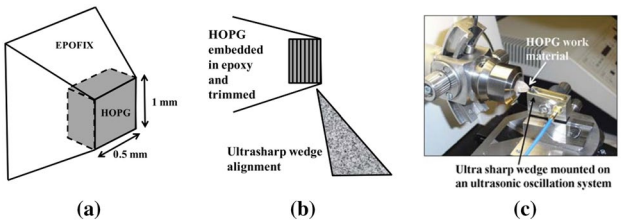

Fig. 16 Novel mechanical cleavage method for graphene synthesis: **a** An epofix with embedded HOPG; **b** Alignment of an ultra-sharp wedge; **c** Experimental setup of an ultra-sharp wedge with an ultrasonic oscillation system [76]

ultra-sonication [69]. In this technique, the graphite fragment is removed repeatedly with adhesive scotch tape to eventually unsheathe the graphene layers. The scotch band stretches over graphite crystals and contributes to graphite layers trapping [70]. This methodology requires roughly an external force. 300 nN μm^{-2} for splitting single surface graphite [71]. Before Novoselov et al. [68], Lu et al. [72] first developed a thin multi-layered graphite retaining thickness of approximately 200 nm through mechanical exfoliation technique utilizing AFM tip (Fig. 15) [73]. This approach is, however, not suitable for the mass production required for the industry due to its labor-intensive approach [74].

Jayasena and Subbiah [76] applied a novel mechanical cleavage method for the synthesis of few graphene layers from bulk graphite. They use an ultra-sharp single-crystal diamond wedge in the presence of an ultrasonic oscillation to cleave a highly ordered pyrolytic graphite (HOPG) sample to generate the graphene layers (Fig. 16) [76]. The cleaved graphene layers are subsequently transferred to a substrate of copper or Si/SiO_2 to carry out the characterization process.

5.2 Chemical exfoliation

The chemical exfoliation process consists of suspension production, which changes graphite to graphene, by forming graphene-intercalated compounds (GICs) [73]. Chemical exfoliation is a two-stage system. The interlayer of 'vdw' forces initially reduces to expand the interlayer spacing in a graphite solution through alkaline metal interference and creates GICs [77]. Afterward, graphene is exfoliated by fast heating and sonication with one or several layers. Ultrasonication is utilized for the development of SGO and Density Gradient Ultracentrifugation for the thickness of different layers [78]. Viculis et al. [79] use a process of chemical exfoliation to produce graphene nanoplatelets (GNPs) using potassium alkali metal. Aqua

ethanol (CH_3CH_2OH) dispersion of the GIC resulted in an exothermic impact and established the formation of GNP. Caution should be taken during reactions, because alkali metals react vigorously with water and alcohol, so an ice bath is required during the reaction to dissipate heat [80]. The main benefit for alkaline metals, including potassium, is their smaller atomic diameter and comparatively miniature than the interlayer distribution order, thus suits the spacing of the layer effectively (Fig. 17) [73]. Therefore, utilizing a chemical exfoliation technique for the synthesis of graphene is an essential and distinctive approach since it can generate a large quantity of graphene at lower temperatures. Additionally, it may also be utilized for the production of functionalized graphene on a large scale.

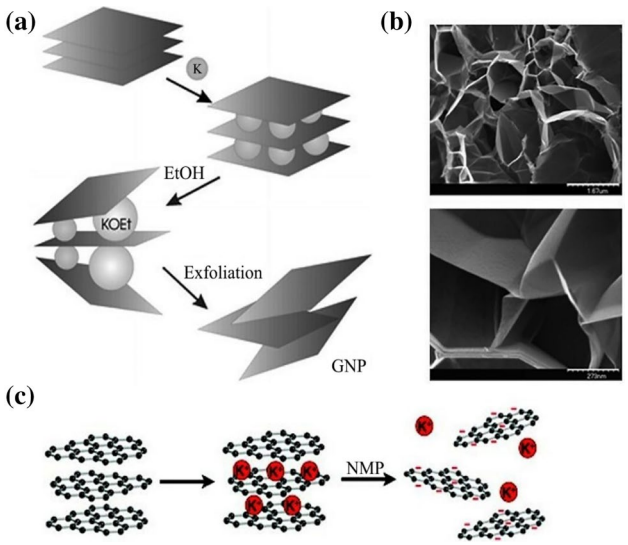

Fig. 17 **a** Chemical exfoliation process using alkali metal; **b** SEM images of exfoliated GNP; **c** Graphene sheet production. Adapted with permission from [81]

5.3 Chemical synthesis

One of the simplest approaches for graphene production is the chemical synthesis approach. Various paper type materials [84], polymer composites [85], energy storage materials, and transparent conductive electrodes already used chemical methods for graphene production [46]. The development of GO from graphite was generally determined using the revised Hummer process, which comprises three stages, i.e., oxidation, purification, and exfoliation [86]. In 1859, B. C. Brodie, the British Oxford pharmacist, researched C:H:O formulations of graphite with a ratio of nearly 2.2:0.8:1 around 169 years ago. Brodie also studied the reactivity of graphite flakes by the application of potassium chlorate ($KClO_3$) and nitric acid (HNO_3) via oxidation treatment [87]. Around 41 years later, Staudenmaier in 1898 strengthens the Brodie process by introducing H_2SO_4 acid to serve as an oxidant [50]. In 1958, Hummers and Offeman discovered a better and quick alternative oxide process for graphite oxide preparation almost 60 years after Staudenmaier [19]. The updated process was used as an oxidizing component by the anhydrous mixture of KMnO4, sodium nitrate ($NaNO_3$), and sulfuric acid-concentrate (H_2SO_4) [88]. Figure 18 illustrates traditional, modified, and improved Hummers strategy for GO fabrication [82]. Tour and his colleagues in the Hummer process recently made progress with the elimination of $NaNO_3$, improved $KMnO_4$ production, and 9:1 mixing ratios of H_2SO_4/phosphoric acid (H_3PO_4) [82]. The benefit of this process is to raise oxidation levels, to improve the structure and its effectiveness, without toxic gas being emitted during oxidation [89]. Figures 5 and 19 reflect the preparation and synthesis of GO nanomaterial [90].

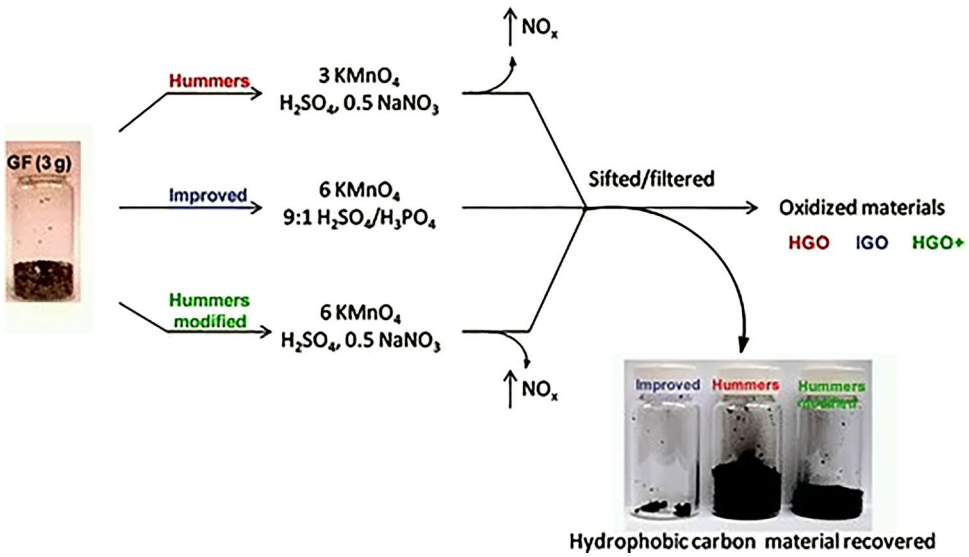

Fig. 18 Higher efficiency of the improved synthesized method was indicated by the small amount of recovered powder. Adapted with permission from [82]

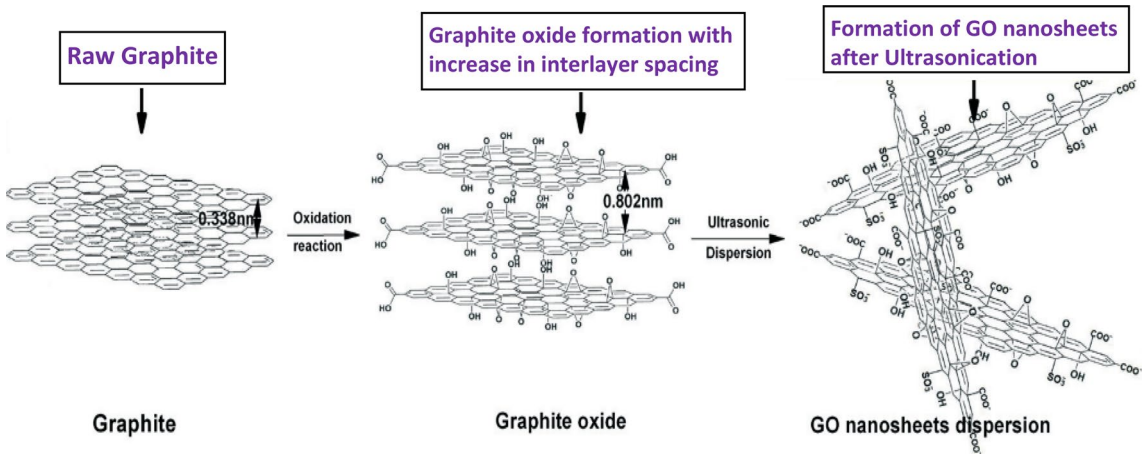

Fig. 19 Schematic presentation of GO fabrication. Adapted with permission from [83]

Table 1 Oxidation methods of graphite-to-graphite oxide adopted by various researchers [91]

Brodie Method (1859)	Staudenmaier Method (1898)	Hummers Method (1958)	Modified Hummers Method (1999)	Improved Hummers Method (2004)
Toxicity: Yes	Toxicity: Yes	Toxicity: No	Toxicity: No	Toxicity: No
Oxidants: $KClO_3$, HNO_3	Oxidants: $KClO_3$ or $NaClO_3$, HNO_3, H_2SO_4	Oxidants: $NaNO_3$, $KMnO_4$, H_2SO_4	Oxidants: $NaNO_3$, $KMnO_4$, H_2SO_4	Oxidants: H_3PO_4, $KMnO_4$, H_2SO_4
C:O = 2.16	C:O = 1.85	C:O = 2.25	C:O = 1.3	C:O = 1.8
Reaction Time: 3-4 days	Reaction Time: 1-2 days	Reaction Time: ~2hours	Reaction Time: ~8hours (6h pre-ox. + 2h ox.)	Reaction Time: 5 days
Interlayer Spacing: 5.95	Interlayer Spacing: 6.23	Interlayer Spacing: 6.67	Interlayer Spacing: 6.9	Interlayer Spacing: 8.3
Limitations: 1. Weak Toxicity 2. Soft dispensability in basic solution. 3. Small size 4. Limiting thickness 5. Imperfect Structure	Limitations: 1. Time Consuming 2. Hazardous approach 3. Formation of Inert gas (CO_2) 4. High risk of explosion 5. Harmful Chemicals	Advantages: > Higher degree of Oxidation > High Yield > Medium performance Limitations: > Incomplete Oxidation > High defects in structure > Used of harmful chemicals. > Lower conductivity. > Not environment friendly.	Advantages: > Improved level of Oxidation. > Higher Performance. Limitations: > Tedious Process (Separation and Purification) > Highly time consuming	Advantages: > Reduced defects in Basal Plane. > Larger amount of oxidized graphite. > Higher conductivity. > Higher Performance. > No toxic gases generated. > Environment friendly. > Coherent structure .

Furthermore, different researchers adopted diverse methodologies for the chemical synthesis of graphite oxide. Table 1 illustrates a comparative summary for each adopted approach based on oxidants, reaction time, interlayer spacing, carbon–oxygen ration, toxic nature, advantages and limitations [39]. Presently, Hummer's and Offeman modified method is the most widely adopted procedure to prepare GO from Graphite Powder. The procedure involved in the fabrication of GO is described as follows [46].

To prepare GO, 2 g of graphite and 1 g of $NaNO_3$ were blended in cooled concentrated 46 ml of sulfuric acid and constantly stirred in an ice bath for 45 min. Further, 6 g of $KMnO_4$ was added gradually to the obtained mix with gradual stirring and cooling. Owing to the strong oxidation reaction causes the instantaneous change in the color of the solution from black to greenish-black under the controlled temperature of 10–15 °C accompanied by the stirring process for 15 min. The obtained solution is maintained at room temperature as its color changes to brown. The reaction mixture was then stirred at 40 °C for 30 min causing the formation of a dense solution. Thereafter, 80 ml of de-ionized water was included, supported by an additional 90 min mix at 90 °C. After that, an additional 200 ml of water added to stop the oxidation reaction. Sequentially, H_2O_2 (6 ml) with a 30% concentrated solution was incorporated into the obtained paste for removal of the excess $KMnO_4$ and terminate the reaction. The complete removal of $KMnO_4$ indicated by a change of color into yellow. The obtained solution was then rested for the complete night duration and detached for the attainment of GO. It was then cleaned with 10% of HCl solution for eliminating the sulfate and other impurities. Afterward, for obtaining the Graphite Oxide the resultant solution was purified and treated with de-ionized water ten times. The resultant solution was then diffused in 100 ml of water and subsequently, ultrasonicated for 1 h to exfoliate the layers and centrifuged for 20 min at 4000 rpm.

A brownish-black GO nanosheets dispersed aqueous solution was obtained with 4 mg/ml concentration that may further dried to powder state at room temperature.

6 Advantages and limitation of top–down approach

For the above-discussed top–down fabrication approach, its advantages and limitations are summarized in Table 2.

7 GO structures

GO has remained undefined in its precise chemical structure and there is no ambiguous model even today. The variation in the GO chemical structure mainly depends on graphite material complexity (sample variations), oxidation conditions, different synthesis approach, the degree of amorphous, and nonstoichiometric atomic composition [96, 97]. Owing to the above drawbacks, several structural models have been proposed by various former researchers through their considerable efforts to understand the structure of GO. In the year 1939, Hofmann and Holst, recommend the first elementary model of GO, which consists of only epoxy groups, bonded on the planar graphene layers [98]. In 1946, Ruess proposed a modification of Hofmann's model, also including the hydroxyl groups to the basal plane and ether-oxygen functionalities, which were randomly distributed on the carbon structure. Scholz and Boehm presented a new corrugated carbon backbone structure in 1969, which was bonded only with carbonyl and hydroxyl groups [99]. Nakajima and Matsuo proposed a model in 1994 [100], having GO comprising of two carbon layers connected to each other by sp^3–carbon–carbon bonds vertically to the layers on which carbonyl and hydroxyl groups were available in relative amounts. Presently, the most renowned GO model was the one developed by Anton Lerf and Jacek Klinowski in year 1996 [101], based on Nuclear Magnetic Response (NMR) spectroscopy for the characterization of GO material. In its proposed model, it was considered to have an unpredictable distribution of flat aromatic regions of non-oxidized benzene rings, and wrinkled areas of alicyclic six-membered rings with hydroxyl and ether groups. Further, in 1998, Lerf and Klinowski [102] revisited their previous model, adding carboxyl groups only on the edges of the GO material. Recently, Szabo and Berkesi proposed a new structural model in 2006. The model comprises a carbon network on two different sides i.e., trans-linked cyclohexane with flat hexagonal connections of C=C bonds and functional groups comprised of hydroxyl, ether, carbonyl, and phenolic groups [103, 104]. Figure 20 represents the foregoing chemical structural model of GO proposed by researchers as discussed above [105].

Several essential structural properties of graphite oxide have been characterized based upon earlier investigations; however, a clearer image of the fine GO structure is needed [106]. As an essential difference, the graphene sheet is made up exclusively of trigonally bound sp^2 carbon atoms [109] whereas the GO sheet has a hexagonal ring based carbon structure with mostly sp^2-hybrids carbon atoms and partially sp^3-hybrids carbon atoms with oxygen-based functional oxygen groups (Fig. 21) [103, 108]. Such as –OH (hydroxyl), –C–O–C– (epoxide), –COOH (carboxyl), and –COO (carbonyl). Among them, sp^3-hybridized cluster including –OH and –C–O–C– on the basal plane whereas, the edges portion

Table 2 Advantages and limitations of fabrication techniques in top-down approach

Synthesis technique	Advantages	Limitations	References
Mechanical exfoliation	Simple process with lesser complexity High quality and purity Well suited for graphene research Lesser defects Easy sample preparation	Time consuming Low production Not suitable for large-scale process Low yield	[92, 93]
Chemical exfoliation	Faster approach Easy and safe process High yield Greater quality and purity Larger size graphene sheet Scalable to industrial level	Larger defect density Lower electrical conductivity Lower concentration Use of harmful chemicals Longer sonication period	[91, 94]
Chemical synthesis	Most used method Larger scale production Scalable to industrial level	Medium quality Large production of liquid waste Higher impurities and defects Lower electrical conductivity Longer synthesis Time Laborious process Additional chemical costs	[31, 95]

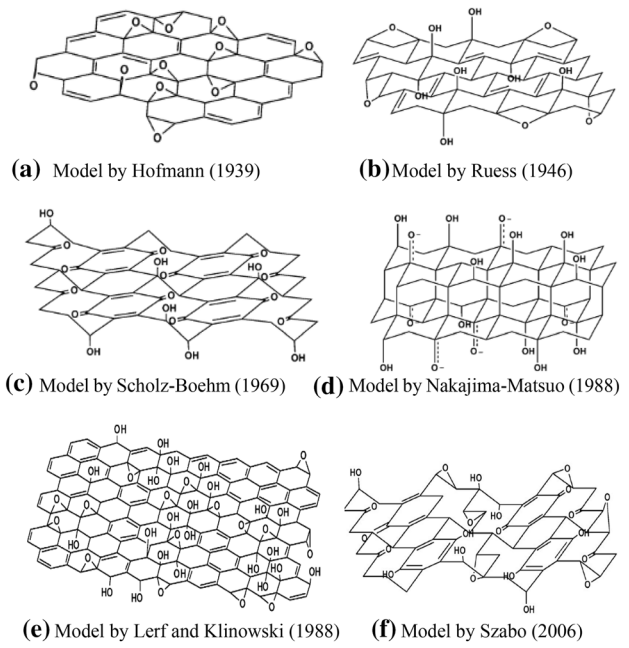

Fig. 20 Summary of several previously proposed chemical structural models of GO. Adapted with permission from [105]

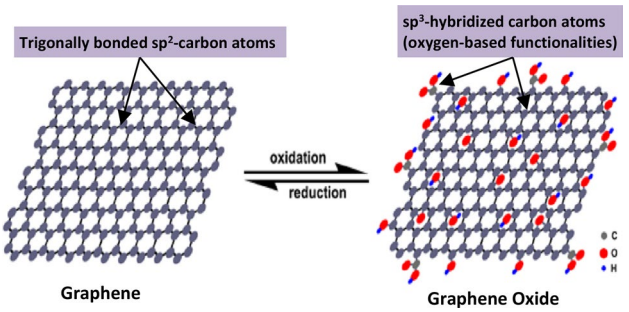

Fig. 21 Schematic structure of graphene and GO. Adapted with permission from [106]

consists of –COO and –COOH groups (Fig. 5) [109, 110]. The hybridized sp^3 carbon atoms are positioned evenly, but arbitrarily, above or below the graphene plane [111]. For further analyzing the structural behavior of GO, numerous microscopic and spectroscopic characterization methods are adopted to explore its diversified structural features (in Sect. 8).

8 GO characterization techniques

Different methodologies for characterizing GO nanomaterial have been implemented based on the evaluated literature. This technique includes X-ray diffraction (XRD), Raman Spectroscopy, Atomic Force Microscopy (AFM), X-ray Photoelectron Spectroscopy (XPS), Fourier transform infrared (FTIR), Transmission Electron Microscopy (TEM), Scanning Electron microscopy (SEM), Thermogravimetric Analysis (TGA), Nuclear Magnetic Resonance (NMR), and Ultraviolet–Visible Spectroscopy (UV–Vis) [112]. The details of these characterization techniques have been discussed in previous research articles [30, 36, 44, 113–115] However, different researchers have adopted different techniques according to their required analysis. Very few researchers have adopted all the above-mentioned techniques for the characterization of GO on a mono sample. The complex structure of GO makes it difficult to suggest a standard characterization approach because, for different applications, different characteristics are essential. However, the basic parameters, which are most relevant to all studies, include the presence of functional groups, degree of disorder or defects in its structure, stacking, and lateral dimension. FTIR and XPS represent the presence of functional groups. Raman spectroscopy indicates the defect or disorder in its structure by relating the intensity of D and G band peaks. SEM, TEM, and AFM illustrate the lateral dimension of GO sheets. Table 4 summarizes the diversified characterization techniques adopted for GO analysis. The following section examines the typological methods of characterization used in literatures and addresses their strengths and limitations. The SEM, TEM, and AFM techniques are essential to the analysis of morphology (shape, shape, structure) and sample dimensions.

8.1 SEM technique

SEM has been employed by several researchers as the strategy for morphologically characterizing GOs because of the ease in preparation of the specimen. Shahhriary et al. [116] noted that the synthesized GO consists of a layered ultra-film frame that folds in space (Fig. 22). Similar analyzes of the graphene sample and the GO were conducted by Karimine-jad et al. [117] (Fig. 23) and identified the bare and smooth GNP layer without curvature (Fig. 23a). Alternatively, GO results in packed nanoplatelets where the functional groups comprising oxygen are similar to high surface roughness. However, the study conducted using SEM techniques must

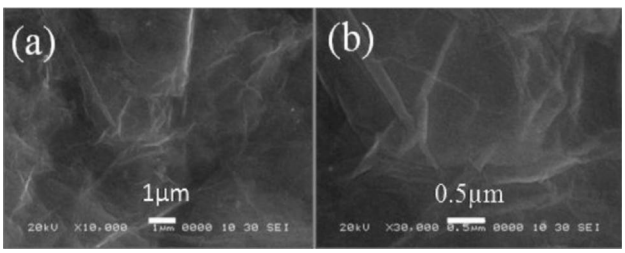

Fig. 22 SEM photographs of GO [116]

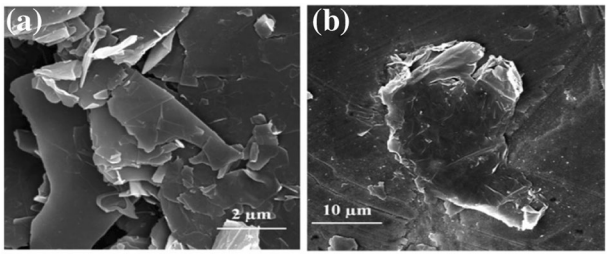

Fig. 23 SEM image of **a** graphene and **b** GO. Adapted with permission from [117, 119]

be performed carefully as improper handling may result in inaccurate data and misunderstanding of the obtained outcome. Shalaby et al. [118]; has described one of the major limitations of the SEM method, that it wholly relies on the obtained visual information which may not impart the complete description of the entire sample because of the confined area and examined particle size.

8.2 TEM technique

TEM imaging is the best tool to view nanoscale material at an atomic resolution [120]. Through converting the electron beam into the imaging lenses and detector, the very thin specimen produces an extremely magnified image when the electrons interact with the samples [121]. Since graphene and GO thickness are only one dense atomic surface, TEM methodology appears to be a crucial and effective way of visualizing its characterization [122]. TEM technique is also applicable to the perception of nanomaterial morphology includes carbon nano tubes and graphene, but the single image obtained may not express the substance it observed [123]. TEM technique is also applied to perceive the morphology of nanomaterials includes Carbon Nano Tubes and graphene, however, it has been observing that the single obtained image may not be able to express the material [124]. Therefore, the TEM imaging technique is used in combination with alternative techniques such as XRD, AFM, and Raman Spectroscopy for characterizing the graphene because of size, layers, type, and inter-planar spacing [112, 125]. TEM analysis has been performed on specimens (Fig. 24) [117] in which the width of the individual GNPs ranges between hundreds of nanometers and ten micrometers, and is more visible compared with the nanoplates after oxidation, due to the presence of oxygen functionalities.

Zhao et al. [126] has implemented the TEM analysis for observing the graphene structure. Additionally, utilizes the TEM result in combination with XRD for the analysis of layers thickness and the inter-planar distances (Fig. 25).

Yang et al. [127] evaluated the morphology and size of the GO using the TEM and AFM imaging technique and found the measured thickness between 2 and 3 nm as shown in Fig. 26.

Recently, high-resolution TEM (HR-TEM) was used to get direct imaging of atomic structure and topologic defects in monolayer GO [128–130]. This marks a major achievement in the exploration of the GO structure. The atomic properties of graphene and single-layer GO were determined by Erickson et al. [128] and had three major sections: holes, graphitic areas, and disordered areas with oxygen functionalities. The estimated area percentages for holes (blue), graphitic areas (yellow), and disordered areas representing oxygen functional groups (red) are in the proportion of 2%, 16%, and 82%, respectively (Fig. 27) [128]. Due to carbon monoxide (CO) and carbon dioxide (CO_2) releases during severe oxidation and sheet exfoliation the hole in the GO was expected to form, generally under 55 nm^2 [131]. In addition, it was proposed that the graphitic areas arise from incomplete basal-plane oxidation with retained honeycomb graphene structure. The disordered regions of oxygen functional groups on the basal plane forms a continuous network throughout the GO sheet [128, 132].

8.3 AFM technique

AFM technique will effectively assess the surface thickness at the nanometer scale [133]. GO thickness and layer number are determined by the AFM process. The thickness of an exfoliated specimen of GO was found to be consistent and almost one nm (Fig. 28) [133]. Stankovich et al. [109] synthesized graphite oxide via Hummer's method exfoliated it and then deposited it onto the different substrates (Si/SiO_2) and highly oriented pyrolytic graphite (HOPG). Using the AFM technique, explained that GO sheets have lateral dimensions of 100–5000 nm and heights in the range of 1.1–1.5 nm (Fig. 29).

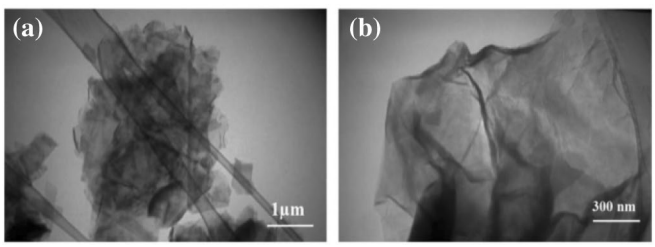

Fig. 24 TEM image of **a** graphene; **b** GO. Adapted with permission from [117, 119]

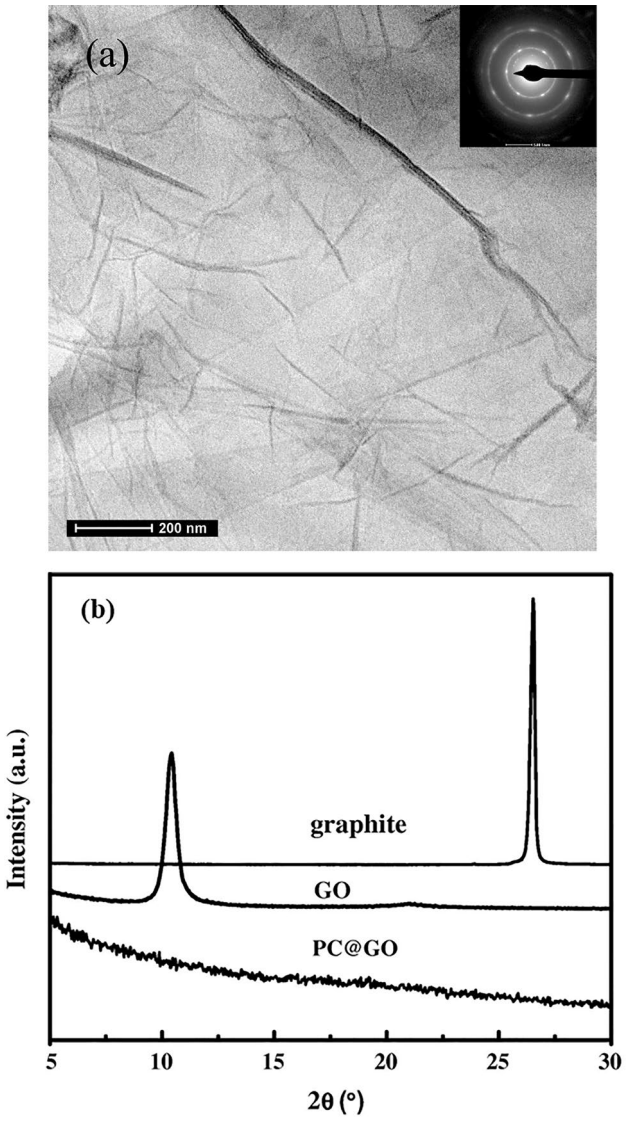

Fig. 25 GO characterization: **a** TEM image; **b** XRD analysis. Adapted with permission from [126]

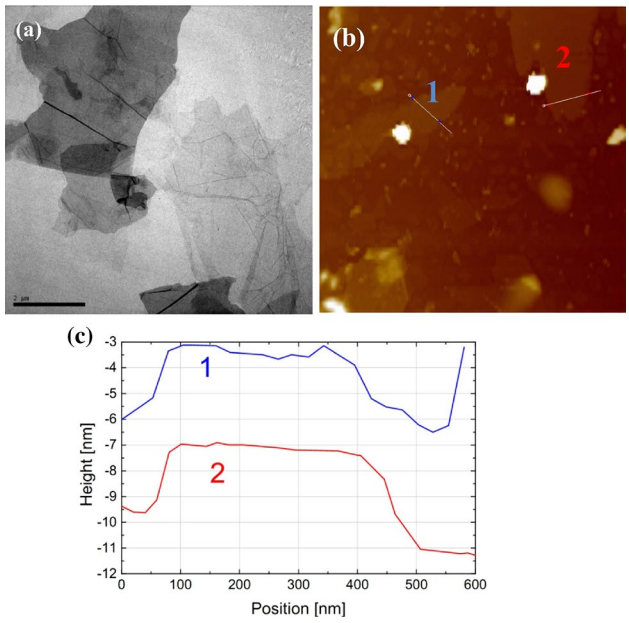

Fig. 26 **a** TEM image of GO; **b** AFM image of GO, where it is plotted two different scan lines for determining the GO heights. Adapted with permission from [127]

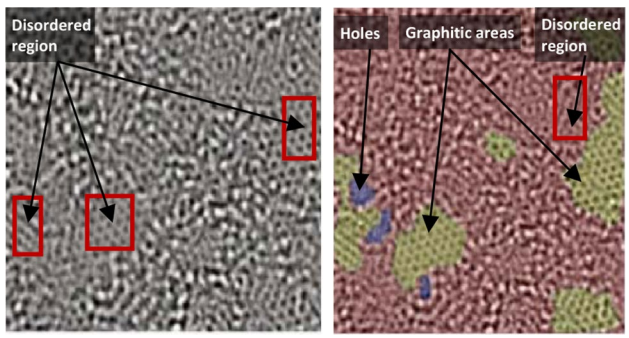

Fig. 27 HR-TEM image of GO monolayer. Adapted with permission from [106, 128] (Blue—holes; yellow—graphitic areas and red—disordered region)

Paredes et al. [134] have successfully revealed the thickness of the sheet using the AFM technique. In his experiment, he observed the thickness of unreduced GO about 1.0 nm and for chemically reduced GO about 0.6 nm. The contrast in the thickness was appeared due to the hydrophilic difference, which occurs in the presence of various functional groups of oxygen (Fig. 30). This technique has also been further examined regarding the mechanical behavior of graphene in parallel to the imaging and thickness detection, as it can resolve the small forces involved in the deformation process. The limitation of this technique includes the complexity in imaging the large area for graphene. Moreover, it's difficult to distinguish in normal operation between the GO and graphene layers using this method, since it only offers topography [112]

8.4 Optical microscope imaging technique

The optical microscope technique is utilized to picture the different graphene layers, as it is one of the affordable, constructive, and easily accessible in laboratories. In this technique, the layer of graphene is placed over an underlying layer of Silicon dioxide (SiO_2) for better imaging visualization. The presence of an underlying layer increases the visibility of the thin sheet [135]. The most common surface

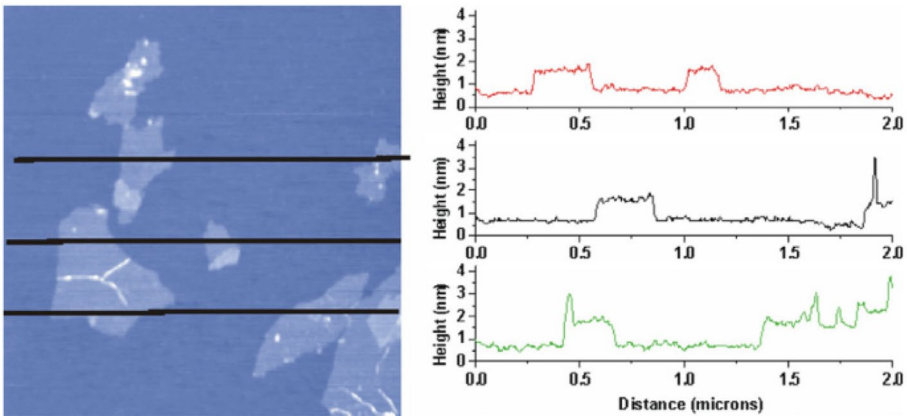

Fig. 28 AFM image of exfoliated GO sheets with three height profiles acquired in different locations. Adapted with permission from [133]

materials used on silicon for increasing the visibility of graphene layers are SiO_2 and Silicon Nitride (Si_3N_4) [136]. Figure 31 represents the image of various exfoliated graphene layers on the substrate of silicon and an overlayer of 300 nm SiO_2. The number of various layers was visualized through different colors and Atomic Force Microscopy (AFM) [137].

8.5 Fluorescence quenching microscopy (FQM) technique

Currently, for instant evaluation of the sample, the FQM technique is adopted to image graphene, GO and reduced graphene oxide (rGO). This approach improved the synthesis process over optical microscope imaging technique and is both cheaper and time efficient [138]. This imaging technique implies the usage of dye-coated GO/rGO for sample preparation. The dye coloring can be easily stripped without harming the sheet samples. The quenching of fluorescence occurs due to the transfer of charge from the dye molecule to GO. The transfer behavior is dependent on the chemical reaction among GO and dye molecules [139]. FQM image is presented in Fig. 32 in contrast to the AFM image. FQM method provides the feasibility to envisage the GO/RGO microstructure even on the substrate of plastic. The limitation of this method involves, the addition of dye on the surface of graphene, as a result, it restricts the more utilization of the same specimen.

XRD and Raman Spectroscopy were shown as effective tools for structural characterization of GO.

8.6 XRD technique

XRD testing is among the most useful and easiest technique for GO characterization. Several researchers utilized this method to assess the distance between the surface of GO. In all, the diffractive angle (2θ) was decreased from 26° (graphite) to 9.45°–10.7° (GO). The variance mainly depends on the experimental method and the

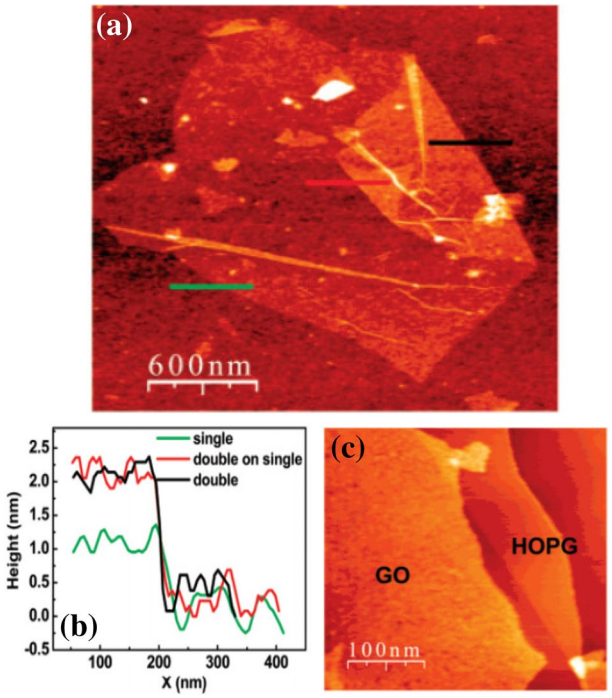

Fig. 29 **a** AFM image on a SiO_2 membrane of a GO monolayer; **b** AFM outlines a single, double, and triple-layer framework; **c** AFM image obtained on a HOPG substrate for a single layer of GO. Adapted with permission from [109]

products used. The interlayer range was raised from 0.34 to 0.94 nm, as a result of the presence of active oxygen-containing groups during the oxidation process [140, 141]. Moreover, it was found that the appearance of GO in an amorphous stage is induced by a slight diffuse dispersion [119] (Fig. 33). Figure 34 presents the obtained XRD analysis of GO and bulk graphite. Owing to the obtained result, the increase in the interlayer spacing of GO is due to the formation of a large number of oxygen-containing functional groups such as hydroxyl, epoxy, and carboxyl between the layers of graphite during oxidation [142]. The

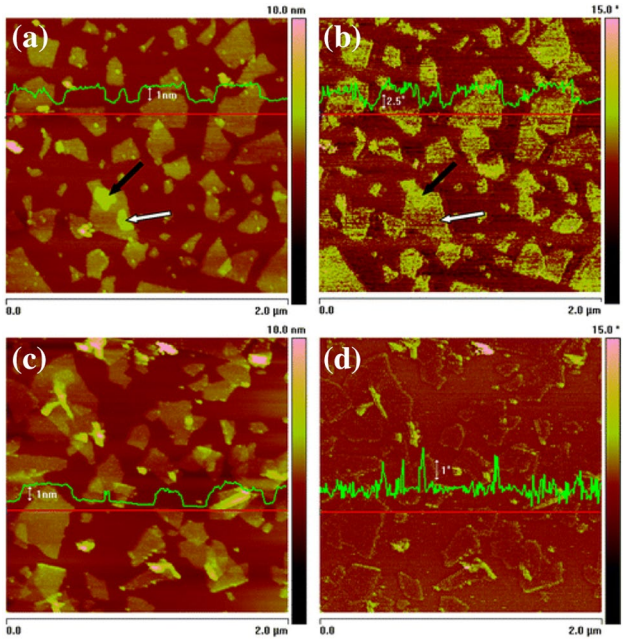

Fig. 30 **a**, **b** Represent the AFM image of non-reduced GO, **c**, **d** represent the chemically reduced GO nanosheets. Adapted with permission from [134]

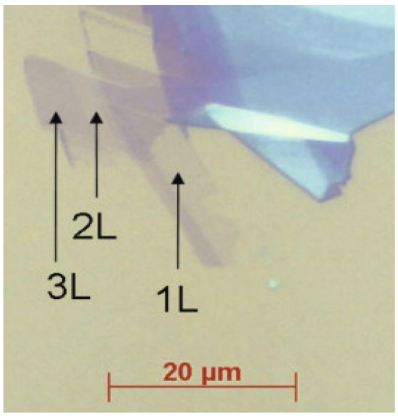

Fig. 31 Optical microscopy analysis for single (1L); double (2L); and triple (3L) layer graphene on Si substrate and over-layer of 300 nm SiO_2. Adapted with permission from [137]

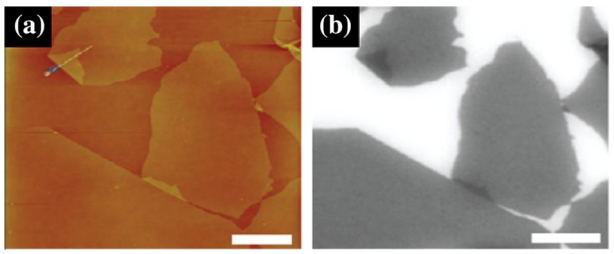

Fig. 32 **a** AFM image displaying monolayer GO placed on a SiO_2/Si substrate; **b** FQM image of the same area, presenting clear similarity to the AFM image. Adapted with permission from [138]

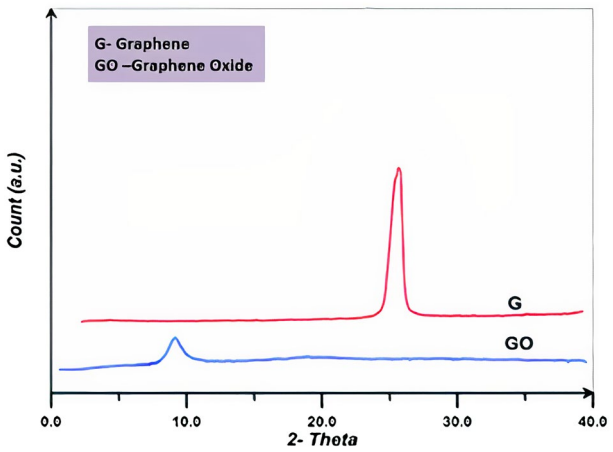

Fig. 33 XRD pattern of graphene and GO. Adapted with permission from [119]

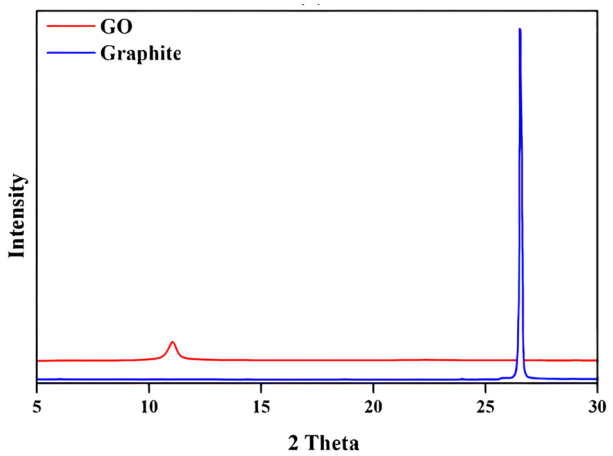

Fig. 34 XRD pattern of graphite and GO. Adapted with permission from [141]

formation of covalent bonding between oxygen and carbon atoms causes an increase in the graphite crystal length [143].

Lv et al. [144], have performed the structural characterization of graphite and GO using the XRD spectra technique (Fig. 35). In his findings, the distance between two layers (d) of GO enlarges to 8.02 nm (dry state) in contrast to that of graphite with 3.38 nm. Figure 35(b) represents the downfall and stretching in the peak intensity of GO. The obtained result signifies the loss in the interaction between graphite layers due to the penetration of oxygen-based functional groups into its inter-layers. This weakens the layers inter-linkage and eases the dispersion of GO in the aqueous solution resulting in the formation of stable nanosheet suspension.

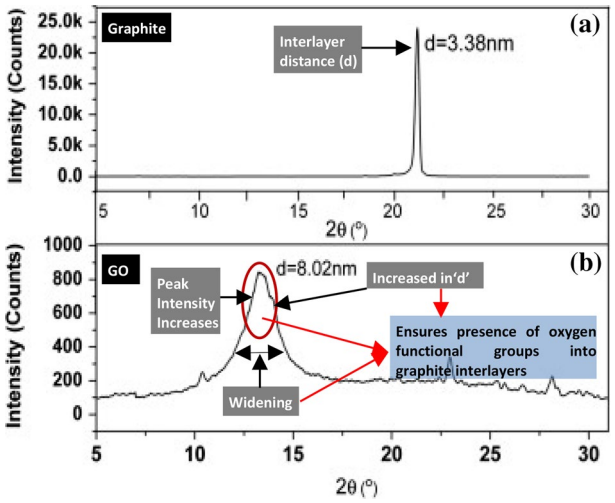

Fig. 35 XRD pattern of (**a**) graphite and (**b**) GO. Adapted with permission from [144]

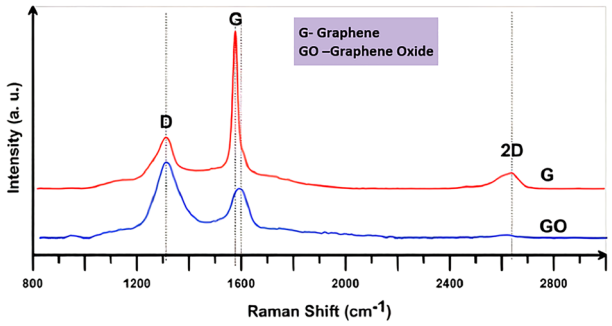

Fig. 36 Raman spectrum for GO and graphite. Adapted with permission from [119]

8.7 Raman spectroscopy technique

Raman spectroscopy is among the most efficient method for characterizing graphene and its derivatives. It is usually very advantageous to measure the order or defects in the crystal structure [82]. The D, G, and 2D band sets of Raman spectroscopy primarily reveals the allotropes of carbon. Because of electron band variations D, G and 2D are about 1350 cm^{-1}, 1580 cm^{-1} and 2700 cm^{-1}, respectively. On recognizing these features, graphene layers characterization is feasible because of the existing number of layers, strain effect, doping concentration, temperature effect, and the presence of defects [145]. The 'D' band (nearly 1350 cm^{-1}) is associated with a structural disorder of sp^3-carbon atoms or structural deficiencies at the borders of the graphene sheet during oxidation process. The G band (almost 1580 cm^{-1}) is linked to the characterization of large crystalline graphite by the in-plane bonding of sp^2-carbon atoms. The 2D or *G′* (about 2700 cm^{-1}) band nearly doubles the D band and is the product of the second-order phase of Raman dispersion [146]. As the number of layers increases, there is a downfall in the relative intensity of the 2D band and a rise in its full width at half maximum value [147]. Using the Raman spectra, many other effects such as thickness calculation, strain results, defects, and doping have also been examined in graphene layers [137]. The structural characterization of the pure graphite and GO was observed via the Raman spectrum [119]. Figure 36 illustrates the presence of the GO band (blue line) and pristine graphite (red line). In the graphite spectrum, the observed three-band includes D band at 1313 cm^{-1}, G band at 1580 cm^{-1}, and 2D-band at 2641 cm^{-1}. The appearance of the D-peak suggests the disordered arrangement of the blue moved G bands (1599 cm^{-1}) in comparison to the graphite. Moreover, XRD method is unable to detect the cement hydration component such as C–S–H gel. So, to overcome this limitation, Horszczaruk et al. [148] utilized Raman spectroscopy method to analyze the GO based cement composites (Fig. 37). In Fig. 37a, the red color graph represents GO based cement composites with formation of two peak bands; D band and G band at intensity ~ 1311 cm^{-1}, 1601 cm^{-1}. The additional curvature that develops in between D and G band ensures the presence of alite (tricalcium silicate) in cementitious matrix (Fig. 37b, c). However, as the saturation level of sample increases with time, there is a downfall in its peak value. Lastly, at 7 days, the peak value of alite (tricalcium silicate) curve completely diminishes under the influence of D and G bands and the curve intensifies with formation of hydration component (Fig. 37d).

Raman technique has been widely utilized to analyze graphene structural defects [149]. Beam et al. [150] studied the defects in graphene and categorized them into point, edges, and crystallite border defects. Point defect is the simplest and symmetrically most common form of defect in a graphene structural matrix because of its high localization in real space and wider frequency range. Edge defects indicate one-dimensional defects and can impart the only momentum in the direction perpendicular to the edges. Lastly, the crystallite border defects are considered as 1-D defects and are represented by the defects in the borders of the crystallite structure of grapheme [151, 152]. You et al. [153] analyzed the edge defects in a monolayer graphene sample at a different relative angle of 30°, 60°, and 90° (Fig. 38). The D-band intensity was extensively studied whereas the G-band intensity was uniform over the whole portion of graphene samples. The green arrow signifies the direction of the incident laser in all samples.

In Fig. 38a, the D-band intensity at 30° relative angle on the upper edge is remarkably higher than the lower edge. The atomic structure of the upper edges resembles an armchair pattern whereas the bottom edges to that of a zigzag

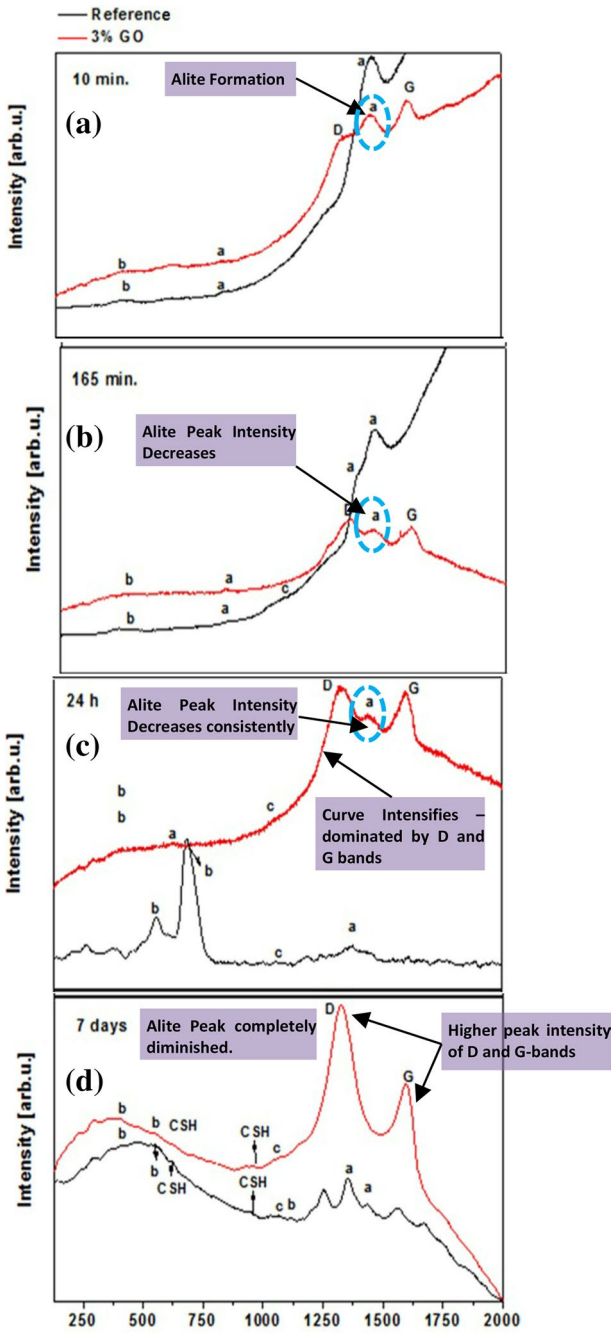

Fig. 37 Raman spectroscopy for GO-cementitious composites and compared with the controlled sample at different time interval. Adapted with permission from [148]

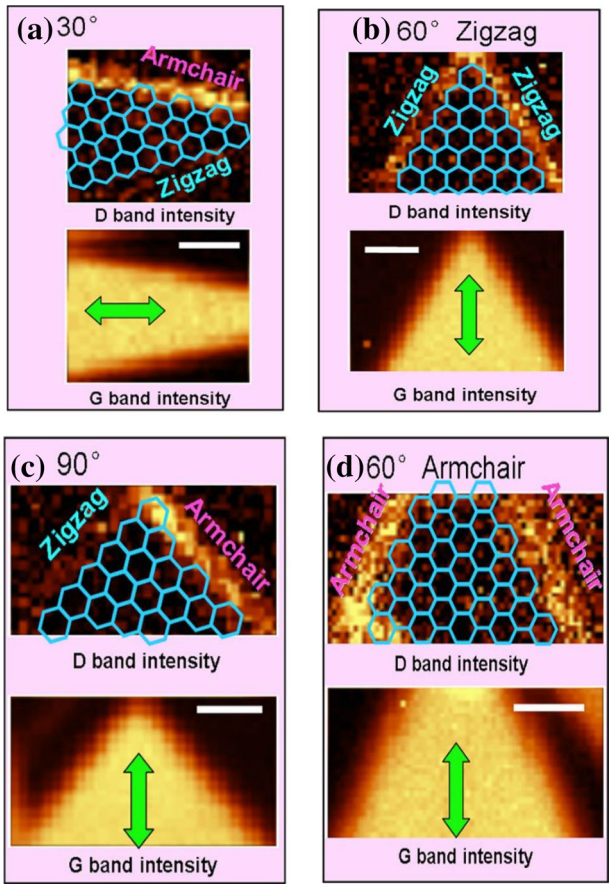

Fig. 38 Raman imaging of single-layer graphene sample at varying relative angles to each other. Adapted with permission from [153]

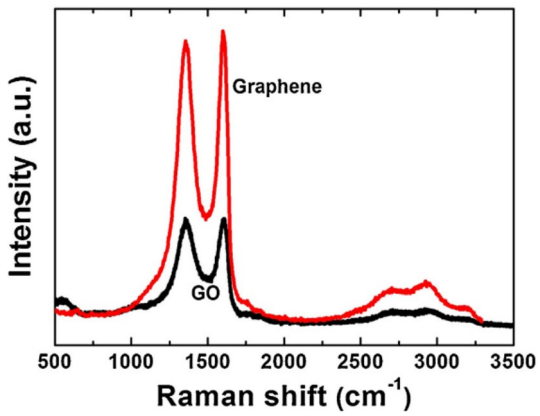

Fig. 39 Raman spectra for graphene and GO. Adapted with permission from [154]

pattern. A similar pattern was observed for the edges at 90° relative angle (Fig. 38c). Figure 38b represents the edges of the graphene sheet at a 60° relative angle. The D band follows a similar zigzag pattern at both edges. This may be due to the identical crystallographic orientation. In Fig. 38d, a similar situation was observed forming an armchair pattern at both the edges at 60° relative angle. The D-band intensity in Fig. 38b was noticeably weaker at the edges as compared to that Fig. 38d. The formation of either armchair or zigzag pattern may be due to the orientation of carbon atoms at the edges. Hence, the edge arrangement patterns may help to predict the orientation of the monolayer graphene sheets.

Moreover, Johra et al. [154] characterized the prepared graphene and GO samples using Raman spectra technique. In Fig. 39, the spectrum for GO characterized as G band (1605 cm^{-1}) and D band (1353 cm^{-1}) whereas for graphene the G band observed at 1600 cm^{-1} that is shifted slightly from the spectra of GO. The observed G-band spectra signifies to the presence sp^2-carbon atoms and D band indicates the disorder intensity that may occur due to vacancies, grain boundaries and amorphous carbon types [155, 156]. In Raman analysis, the intensity ratio (I_D/I_G) determines the quality of product [147]. The I_D/I_G ratio for GO was calculated as 1.00 which was reduced to 0.96 for graphene spectra. The difference indicates the repair of defects or disorder by the aromatic structures. Moon et al. [157] reported an increase in the I_D/I_G ratio for reduced GO when treated with hydroiodic acid (HI) and acetic acid (CH_3COOH). This indicates the presence of large quantity of structural defects for reduced GO structure. Additionally, the 2D band for graphene was observed at 2700 cm^{-1} that indicates the number of graphene layers. Thus, it can be concluded that the prepared graphene contains layers with few defects. The S3 band for graphene was observed at 2900 cm^{-1} that results from the peak combination of D–G band. The S3 band intensity defines the reduction in structural defects that is due to lower oxygen content in graphene layers [158]. The higher peak intensity for graphene as compared to GO indicates better structural graphitization [157]. Thus, Raman spectroscopy technology has been widely preferred for studies of GO dispersion due to its constructive behavior, rapid preparation of the samples, and simplified interpretation of GO distribution.

For thermal degradation stability, evaluation of GO, thermogravimetric analyses (TGA) approach proves to be an essential technique.

8.8 Thermogravimetric analysis (TGA)

Various researchers had examined that the inclusion of graphene and GO, may significantly improve the thermal deterioration stability of polymers, such as epoxy, HDPE, poly(arylene ether nitrile), polycarbonate [159, 160]. To determine the characteristic decomposition temperature of GO and the oxygen functionalities bonded over it, many authors have examined the behavior following the Thermogravimetric Analyses. The observations concluded were almost quite similar:

a. The loss detected at 100 °C, is very minute and occurs due to the disappearance of water molecules.
b. Due to the decomposition of easily altered oxygen groups, loss between 100 and 300 °C was observed.
c. The small increment has been observed in the loss rate for temperature between 300 and 600 °C, due to the separation of most stable oxygen-based functionalities.
d. Beyond 600 °C, the ignition of the carbon firmness has been observed of the GO.

Jeong et al. [161] specifically studied the effect on thermal stability of the oxygen functionalities in GO due to change in weight at temperature from 200 °C increased up to 1000 °C (heating rate@50 °C/min.) for 2 h, 5 h, 6 h, and 10 h, respectively (Fig. 40). In his observation, two major peaks are observed around 240 °C and 650 °C that further dispersed into four on magnification (Fig. 40f). Formation of peak 1 corresponds to water evaporation from the solution. Peaks 2 and 3 attribute to the strong bonding of –OH and –C–O groups whereas Peak 4 occurs due to vaporization of carbon [162] groups. However, the attributed loss of oxygen functionalities is very small, when GO is treated at 200 °C@6 h and even after for 200 °C@10 h treatment more than 15 wt% of oxygen functionalities remains in GO solution. It signifies that the thermal treatment causes only a partial reduction of GO, i.e., some oxygen functionalities had still been survived (Table 3). Based on the above literature analysis, GO validates the potential of having superior thermal stability, proving it to be beneficial for future electronics, energy storage devices, concrete materials, and other applications.

For the chemical characterization of GO, various spectroscopic techniques have been utilized to study the oxygen functional groups bonded randomly on the surface of GO.

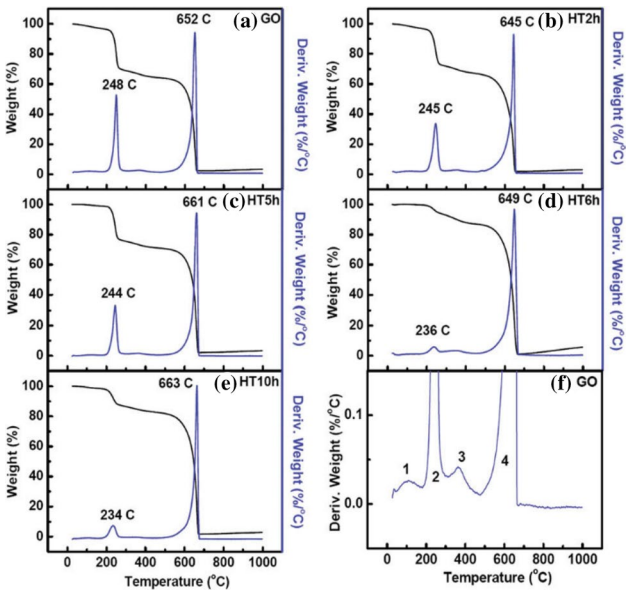

Fig. 40 TGA of; **a** GO treated at 200 °C; **b** for 2 h; **c** for 5 h; **d** for 6 h; **e** for 10 h and **f** GO magnification for peak features. Adapted with permission from [161]

Table 3 Loss in atomic ratio of O:C and water evaporation due to thermal effect [161]

Specimen	O:C (Loss in atomic ratio)	Water evap.
GO	0.39	0.18
GO@2 h	0.34	0.16
GO@5 h	0.12	0.07
GO@6 h	0.10	0.02
GO@10 h	0.10	0.08

The involved techniques include Solid State Nuclear Magnetic Resonance (SS-NMR), X-ray Photoelectron Spectroscopy (XPS), and Fourier Transform Infrared Spectroscopy (FTIR). Compare to XPS and NMR techniques, IR spectroscopy is the most employed technique for the Chemical Characterization of GO. XPS and NMR techniques are determined to be an efficient and strong approach, but its execution is quite difficult and result interpretation is also not easy. Alternatively, IR is simple, rapid, and does not involve sample preparation.

8.9 FTIR technique

A convenient, quick-operated, and non-destructive technique for chemical characterization is infrared spectroscopy (IR). No sample preparation or specific substrates are needed, as opposed to other techniques [163]. IR techniques are focused primarily on correlations between radiation and matter when they contribute to the absorption of radiation in the electromagnetic spectrum. It is used to obtain information on different functional oxygen groups produced during the graphite oxidation process. Figure 41 represents the formation of the GO spectrum and its related functional groups through IR technique [164]. The observed results include the existence of different oxygen functional groups at oscillating modes such as hydroxyl (phenol, C–OH) (3530 cm^{-1} and 1080 cm^{-1}), ketonic (C=O) (1600–1650 cm^{-1} and 1750–1850 cm^{-1}), carboxyl (–COOH) (1650–1750 cm^{-1}), C=C (sp^2 in-plane vibrations) (1500–1600 cm^{-1}), epoxide (C–O–C) (1230–1320 cm^{-1}), and other chemical groups. The overlapping regions mostly include functional groups of ether types (C–O) and ketonic types (C=O) in oscillating range of 850–1500 cm^{-1}. This overlapping portion are categorized into three different zones such as α-zone (900–1100 cm^{-1}), β-zone (1100–1280 cm^{-1}) and γ-zone (1280–1500 cm^{-1}). Functional groups illustrated in different colors includes green spectrum for epoxide groups, red spectrum for C–O, blue spectrum for C–OH, brown spectrum for COOH, grey spectrum for C=O and light blue for C=C groups [164].

Ambra Romani [165] in her research work had mixed the GO in water solution in a beaker and observed that most of the GO tend to segregate at the beaker bottom while others remain in the upper part of the solution. Two different samples of GO were obtained from the same group: One from the segregated portion (GO Down) of the solution at the beaker base and the other from the upper portion of solution (GO Up) at the beaker top and followed the same by the Infrared Spectroscopy analysis for each sample. As per the observations, the two spectra, shown very identical spectral patterns having few differences in the relative intensities of some bands (Fig. 42).

Rise or peaks in the graph has been visualized for both the samples as follows:

a. At 3400 cm^{-1}, a strong and broad absorption, due to –OH stretching modes of hydroxyl groups bonded on the carbon backbone;
b. At 2400 cm^{-1} and 2900 cm^{-1}, two small and broad absorption, making the presence of hydrogen-bonded carboxyl groups;

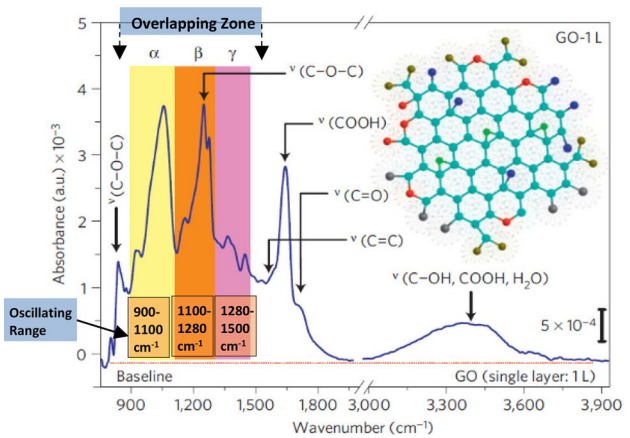

Fig. 41 FTIR spectra of GO. Adapted with permission from [164]

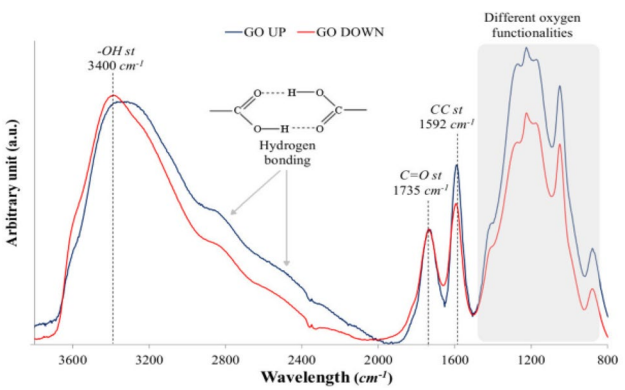

Fig. 42 FTIR spectra of GO Down and GO Up [165]

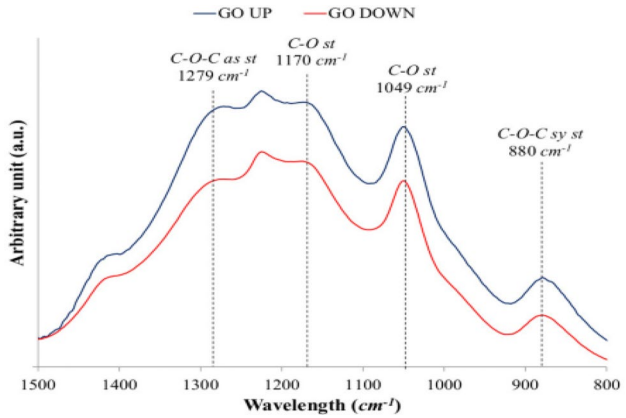

Fig. 43 Magnification of a part of the FTIR spectra from 800 to 1500 cm^{-1} of GO Down and GO Up [165]

c. At 1735 cm^{-1}, C=O stretching of the carboxyl groups bonded on the edges of graphene sheets has been reported;
d. At 1592 cm^{-1}, the stretching of the sp^2 carbon backbone;
e. At 1279 cm^{-1} and 880 cm^{-1}, overlapped bands of C–O–C and C–O stretching had been notified, because of the oxygen functionalities bonded on the carbon backbone.

The band of the IR spectra ranging in between 800 to 1500 cm^{-1} has been further magnified (Fig. 43) [165], for simple identification of the peaks describing the presence of oxygen functionalities in the samples. Thus, concluding the oxidation phenomenon for both GO Up and GO Down.

From the magnification part of the IR spectra, it had been observed that GO Up presents a higher relative intensity for the band of 800–1500 cm^{-1} as compared to GO Down. The above observation signifies, that the GO Up sample had been characterized by a higher amount of oxygen functional groups, whereas, GO Down might be less exfoliated and tends to separate from the solution. There may be other more approaches for characterizing GO nanomaterial such as extended X-ray absorption fine structure (EXAFS) [166, 167], X-ray absorption near-edge structure (XANES) [168], resonant inelastic X-ray scattering (RIXS) [167], electron energy loss spectroscopy (EELS) [169]; however, this review paper covers the most widely used methodologies specifically in the field of civil engineering.

8.10 XPS technique

X-ray photoelectrons (XPS) are among the commonest and most efficient techniques used to examine the chemical surface composition of graphene and their derivatives concerning carbon content (C), oxygen (O), and the binding energy (eV) of functional groups [113, 170]. The calculation of carbon and oxygen in conjunction with elemental testing is a detailed procedure because it is complicated to absolutely dehydrate a GO specimen [82]. The X-ray light that penetrates deep into the sample irradiates the specimen layer in this procedure. Several electrons are, therefore, thrown away and their kinetic energy is further calculated [171]. Toh et al. [172] uses the XPS range to research GO and ERGO characterization and structural advancement. Electrochemically reduced graphene oxide (ERGO) is referred to as electrochemically reduced graphene oxide. The features are different from pristine graphene as it conserves some graphene structures, which preserves some oxygen functions in the carbon basal plane [173]. GO and ERGO XPS spectrum demonstrate the peak development of O_{1s} and C_{1s} at ~ 530 eV and ~ 284 eV binding energy, respectively (Fig. 44) [174]. To determine oxygen concentration in the oxidized graphene, the peak-intensity ratio between O_{1s} and C_{1s} is considered [175]. The spectrum of both O_{1s} and C_{1s} may, therefore, be utilized to assess oxygen components in the backbone of graphene carbon. The GO maximum O_1 spectrum indicates the presence of several functional groups, including C=O (530.4–530.8 eV), C–OH, and/or C–O–C (532.4–533.1 eV) and chemically adsorbed oxygen and/or water (534.8–535.6 eV) [176]. In contrast to one sharp peak, in the C_{1s} graphite spectrum, the high-resolution GO C_{1s} generally show a complex band with two peaks roughly 2 eV apart (Fig. 45a) [134]. The two major peaks are sp^2 and sp^3-carbon with various configurations of C–O linkage. The relative intensities of both peaks vary depending on the oxidation degree [177]. The GO spectrum of C_{1s} was deconvoluted in four individual functional group peaks (C–C or C=C, C–O–C, C=O, COOH) at various binding energies [172]. Furthermore, the bulk of the C_{1s} spectra in the GO comprised of C–O–C functional group with binding

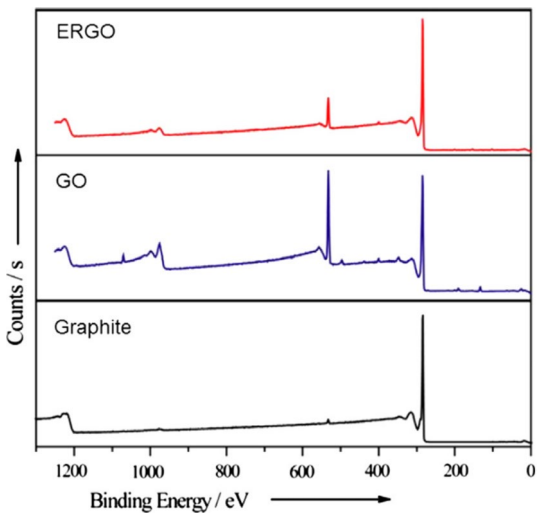

Fig. 44 XPS spectra of graphite, GO, and ERGO. Adapted with permission from [174]

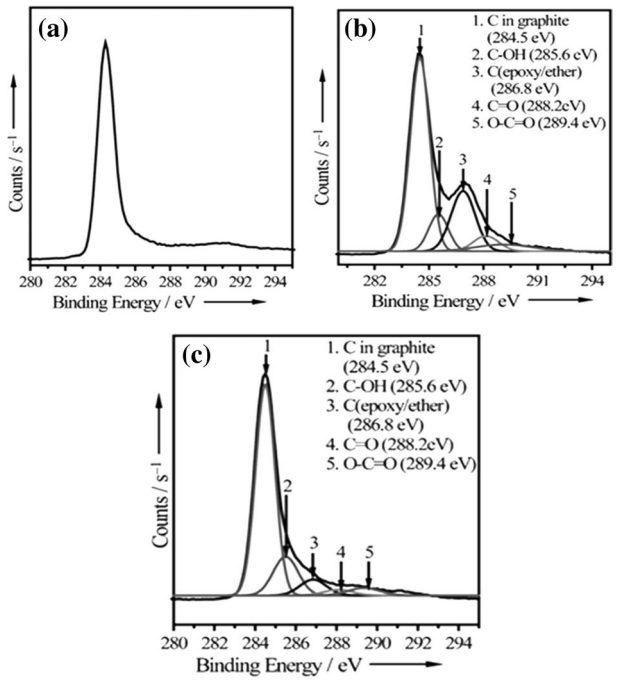

Fig. 45 C_{1s}-XPS spectrum of **a** graphite; **b** GO; **c** ERGO. Adapted with permission from [174]

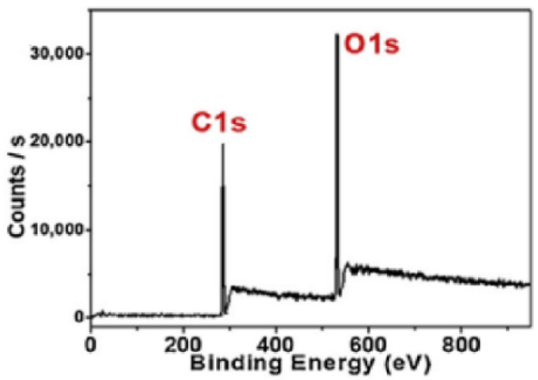

Fig. 46 XPS spectra of GO. Adapted with permission from [113]

energy close to C–OH, although the group may have binding energy within the C=O range (Fig. 45b) [175]. The peak intensity of C–O, C=O, and O–C=O falls to a much lower value with electrochemical reductions (Fig. 45c) [174]. The spectrum of ERGO C_{1s} is comparable to graphite but has a wider band form, indicates that major oxygen functions in GO are eliminated after electrochemical reduction [178]. While the optimum bonding intensity of sp^2 (C=C) rises in the ERGO spectrum of C_{1s}, therefore, revealing that the sp^2 bonded graphene carbon network is partially restored [174].

GO characterization was analyzed using XPS spectrum and high peak intensity for C_{1s} and O_{1s} was observed

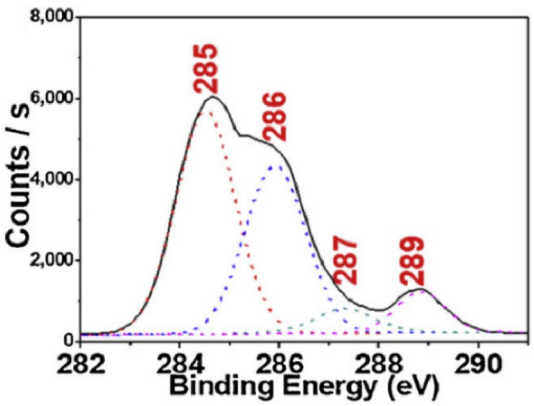

Fig. 47 C_{1s} expanded view indicating the formation of functional groups at different binding energy. Adapted with permission from [113]

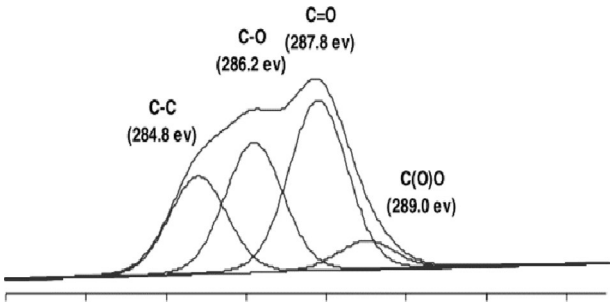

Fig. 48 C_{1s}-XPS spectra of GO. Adapted with permission from [133]

(Fig. 46) [113]. The C_{1s} and O_{1s} elements showed the existence of different functional oxygen groups. The functional groups comprise of C=C/C–C (aromatic rings), C–O–C (epoxide), C=O (carbonyl), and –COOH (carboxyl) with 285, 286, 287, and 289 eV binding energy (Fig. 47) [113].

GO-XPS range illustrates significant deviations from graphene owing to the development of the symmetrical and narrower C_{1s} graphene band into a broad, widened band of two maximums [179]. Figure 48 shows the presence of many functional groups such as C–C, C–O, C=O, and O-C-O with distinct binding energies of ~ 284.6 eV, ~ 286.2 eV, ~ 287.8 eV, and 289.1 eV[133].

Additionally, the level of GO oxidation with the XPS spectrum was researched by Lu et al. [180]. The result states the formation of carbon–oxygen functionalities includes –COOH, C=O, C–O, and –C–C at binding energy 289.0, 288.3, 286.4, and 284.4 eV (Fig. 49). The ratio observed for C:O is approximately two, which indicates a scattered solution consisting primarily of 1 to 2 layers with oxygen functional groups. In a similar study, Xu et al. [181] characterized the GO sample using an XPS

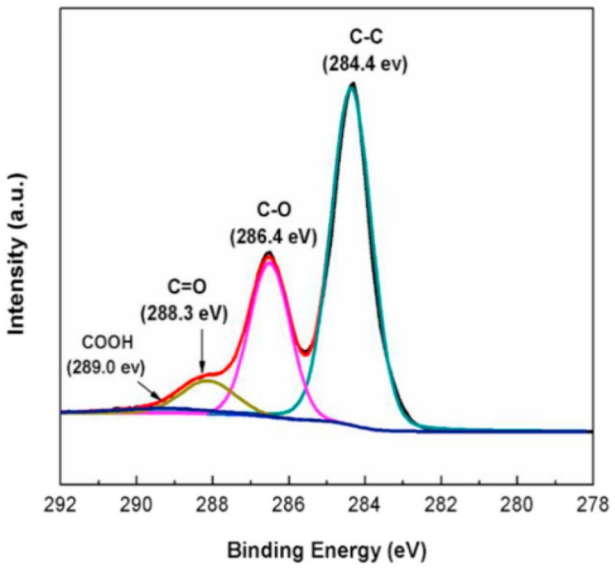

Fig. 49 XPS analysis for GO. Adapted with permission from [180]

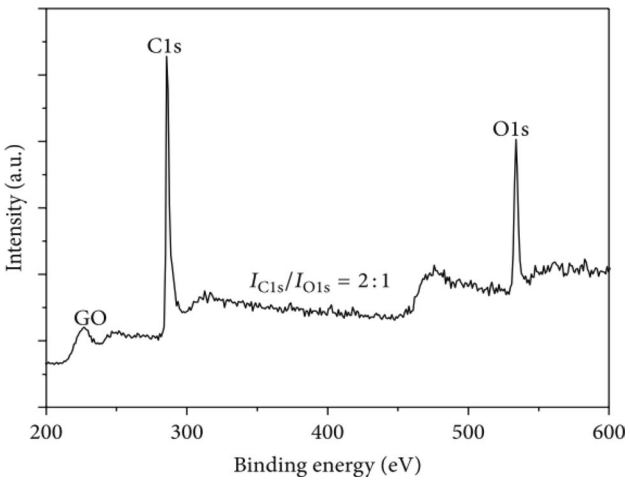

Fig. 50 XPS result of GO [181]

spectrometer. The XPS result states the heavy oxidation of GO for carbon (C_{1s}) to oxygen (O_{1s}) in a ratio of 2:1 (Fig. 50).

Furthermore, Johra et al. [154] also uses the XPS spectrum to evaluate graphene and GO behavior. GO spectrums for the C_{1s} represented three peaks corresponds to sp^2-carbon, epoxides, and carboxyl-functional groups at 284.6, 286.5, and 288.5 eV (Fig. 51) after the deconvolution [182]. Another peak was observed at 287.5 eV for graphene, which suggests the presence of the C=O functional group. With an extremely strong band at 284.6 eV, the XPS spectrum of graphene obtained after a thermally hydraulic reduction is almost twice the peak of GO. In contrast, to GO, the band intensity related to carboxyl, epoxide, or other

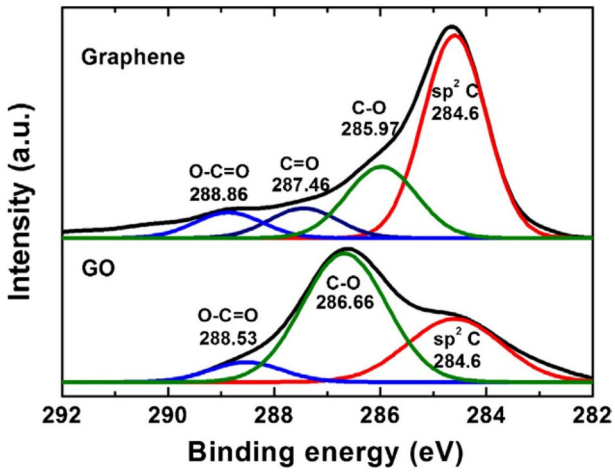

Fig. 51 XPS spectrum of graphene and GO. Adapted with permission from [154]

functional groups had been decreased. In addition, there were no elements other than C and O in the XPS graphene spectrum, which indicated the lack of any impurities [180].

8.11 NMR Spectroscopy Technique

Nuclear Magnetic Resonance (NMR) spectroscopy is a non-destructive and analytical technique in the quantitative and structural determination of nanoscale materials [183]. It provides detailed information about the chemically reactive environment surrounding the magnetically active nuclei of the respective nanomaterials [184]. With a net magnetic moment ($I \neq 0$), the nuclei is coupled with an angular momentum in a unilateral direction (I is the spin quantum number of the nucleus). The influence of extrinsic magnetic field promotes the precession of nucleus around it. As all the nuclei, precess about the extrinsic magnetic field this process generates a quantifiable oscillating signal used for NMR spectroscopy (Fig. 52) [185–187]. NMR method may be utilized in any nucleus that has an odd number of protons or neutrons, or both [(for example, hydrogen nuclei (1H), carbon (13C), phosphorus (31P), etc.]). The magnetic moment of hydrogen is relatively substantial ($\mu = 14.1 \times 10^{-27}$ J/T) and is, therefore, applied in NMR studies [188]. The hydrogen nucleus consists of a single proton (+ ve charged), which may be seen as a current loop that generates a magnetic field as shown in Fig. 53 [188, 189].

Solid-state ^{13}C-NMR spectroscopy is a unique tool that can provide site-specific structural information for all carbon nanostructures [190]. ^{13}C-NMR chemical shifts are highly sensitive in nature and helps to identify the morphology of carbon-based nanomaterials, such as structural defects, impurities and functional groups [191]. This method is also advantageous in removal of any sort of paramagnetic

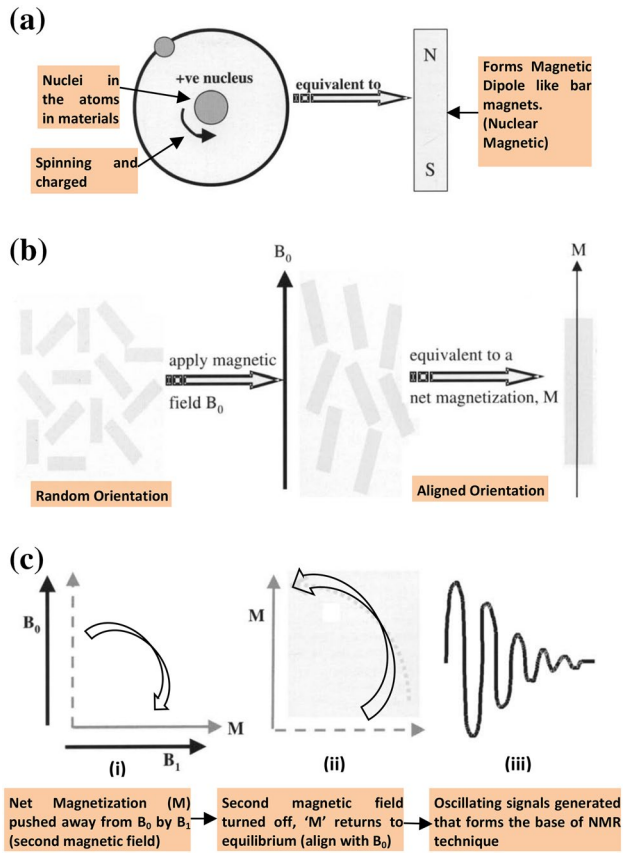

Fig. 52 Nuclear Magnetic Resonance (NMR) technique. Adapted with permission from [134]

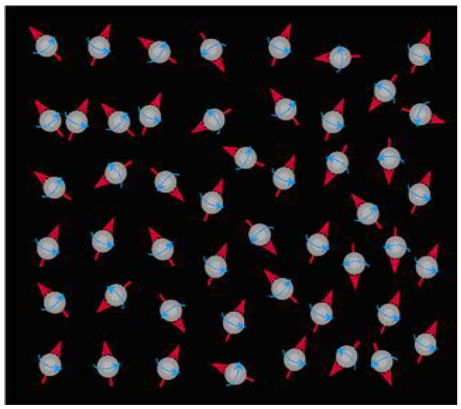

Fig. 53 Randomly arranged hydrogen nuclei [189]

impurities and improve in structural sensitivity of carbon nanostructure [190]. Solid-state ^{13}C-NMR spectroscopy is a considerably efficient method of examining the GO chemical structures [192]. The most recognized and familiar GO model is the one obtained by Lerf and Klinowski using the NMR spectroscopy (Fig. 54). It indicates that GO structure

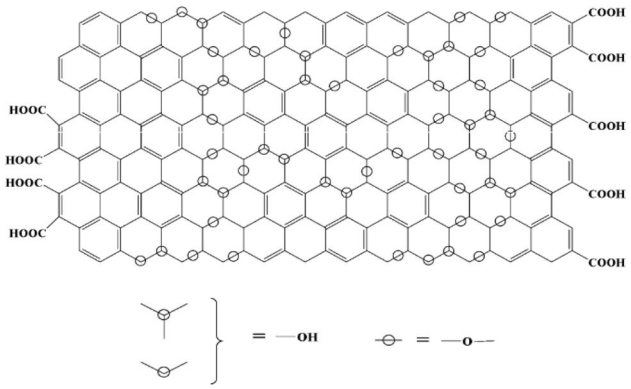

Fig. 54 GO-structural model developed by Lerf–Klinowski. Adapted with permission from [102]

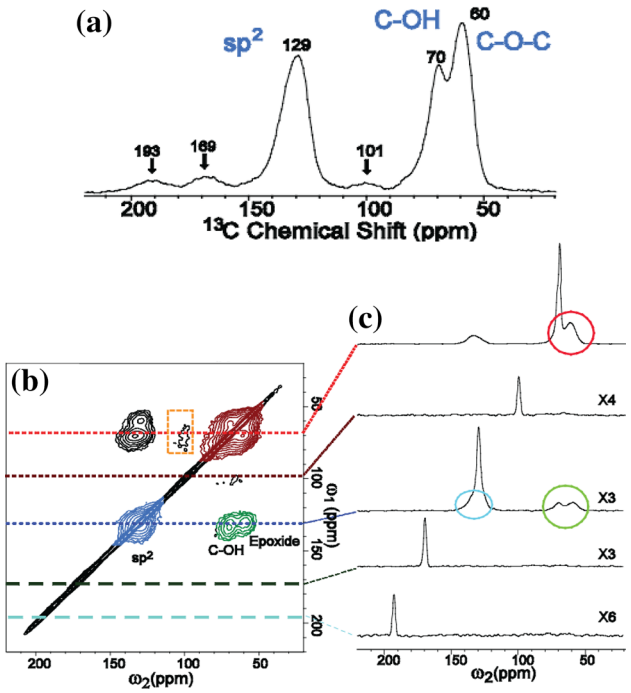

Fig. 55 High-resolution solid-state NMR for graphite oxide characterization; **a** 1D-^{13}C MAS spectrum; **b** 2D-^{13}C chemical shift correlation NMR spectrum; **c** selected 2D spectrum at intensity 70, 101, 130, 169 and 193 ppm in ω_1 axis. Adapted with permission from [193]

includes aromatic areas with un-oxidized benzene rings and the six-membered aliphatic ring comprising –OH, –C–O–C, –COO, and –COOH functional groups [102]. This was one of the most revolutionary research in characterization of GO as the previous models relied primarily on elemental composition, reactivity and X-ray diffraction studies [101].

High-resolution solid-state ^{13}C-NMR utilize magic angle spinning (MAS) method to characterize GO at the molecular level. Figure 55a show 1D-^{13}C MAS spectrum

[193]. The three major peak represents functional groups such as epoxide (59.7 ppm), C–OH (69.6 ppm), and sp^2 hybridized ^{13}C (129.3 ppm). Figure 55b illustrates 2D-^{13}C chemical shift correlation NMR spectrum of graphite oxide that was prepared using a modified Hummer's method with ^{13}C-labelled graphite. It helps to identify ^{13}C–^{13}C pairs that are directly bonded or separated by two bonds [193]. The cross peaks were observed at the positions (ω_1, ω_2) in ppm. For green spectrum two cross peaks noted at 133 ppm, 70 ppm and 130 ppm, 59 ppm (Fig. 55b). The cross peaks represent sp^2-carbon observed at ~ 130 ppm (ω_1), C–OH groups (70 ppm, ω_2) and epoxide groups (59 ppm, ω_2). The relatively higher intensities of cross peak illustrates the formation of strong bonding of sp^2–^{13}C to C–OH ^{13}C and epoxide-^{13}C [194]. Similarly, the red signal illustrates strong bond formation in between ^{13}C-OH and ^{13}C-epoxide. The blue spectrum indicates the presence of sp^2-^{13}C groups and bonded with each other. The minor groups cross peaks are highlighted in orange box at 101 ppm [105, 193]. It was concluded that for analysing chemically modified graphene, using solid-state ^{13}C-NMR spectroscopy technique is a constructive and precise approach [103]. However, due to its limitations such as lower sensitivity, high magnetic field requirement, difficulties in execution and result interpretation [195] makes its lesser effective as compare to other available techniques, particularly in construction materials domain.

Figure 56 illustrates the NMR spectrum of graphene and GO [154]. The spectrum peak intensity centered at 130 ppm signifies the sp^2 C=C; at 59 ppm for C–O–C; at 167 ppm for C=O and around 68 ppm corresponds to –OH groups [196]. However, after reduction the spectrum peak at 59, 68 and 167 ppm disappeared whereas 130 ppm reduces to 117 ppm which attributes to the modification in behavior of sp^2 C=C [133].

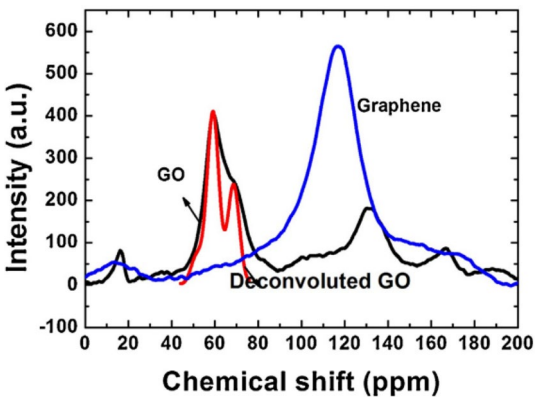

Fig. 56 NMR spectrum of graphene and GO. Adapted with permission from [154]

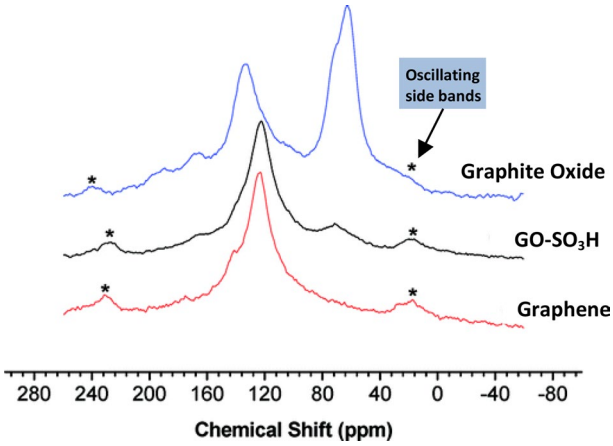

Fig. 57 NMR spectrum of graphite oxide, GO-SO_3H and graphene at 90.56 MHz and 9.4 k rpm. Adapted with permission from [197]

Figure 57 demonstrates the solid-state ^{13}C-NMR spectra (90.56 MHz and 9.4 k rpm) for graphene, sulfonated graphene oxide (GO-SO_3H) and graphite oxide [197]. For graphite oxide two distinct spectrum is visualized. The spectrum peak at 134 ppm attributes to sp^2 C=C and the other at 70 ppm signifies hydroxylated carbon groups. At 167 ppm, a weaker spectrum is observed which indicates the existence of –COO groups [198]. Furthermore, after reduction to GO–SO_3H and graphene, the peak spectrum at 70 ppm and 167-ppm fades off, the spectrum at 134-ppm shift to 123 ppm and a minute spectrum emerges at 140-ppm. The rise in small peak spectrum corresponds to covalently bonded carbon groups [133, 199].

9 Summary of GO characterization methods

Various methodologies for the characterization of GO nanomaterial have been used based on reviewed literature. These techniques include XRD, Raman, AFM, XPS, FTIR, TEM, SEM, TGA, UV–Vis, and NMR. However, different researchers have adopted different characterization techniques according to their required analysis. Very few researchers have adopted all the above-mentioned techniques for the in depth characterization of GO on a mono sample. Therefore, it is very difficult to recommend any particular characterization technique as a standard method. Table 4 represents the mapping summary of the diversified characterization techniques adopted for GO analysis in last 11 years (2010–2021). For better-refined study, 150 literature samples were examined, assessed, and classified based on their utilization percentage (U).

Table 4 Mapping summary of GO characterization techniques in last 11 years (2010–2021)

Year	XRD	Raman	AFM	XPS	FTIR	TEM	SEM	TGA	UV–Vis	NMR	References
2010			▲					▲			[200]
							▲				[201]
	▲			▲		▲				▲	
		▲				▲					[202]
	▲								▲		[203]
		▲				▲				▲	
	▲		▲			▲		▲		▲	
		▲		▲		▲		▲		▲	
		▲		▲			▲			▲	
		▲									[204]
2011	▲				▲			▲			[205]
		▲		▲		▲			▲		[174]
			▲								[206]
		▲			▲		▲		▲		[207]
	▲			▲		▲		▲		▲	
	▲		▲		▲			▲			[209]
2012	▲						▲				[210]
			▲			▲				▲	
		▲		▲		▲				▲	
						▲			▲		[145]
		▲			▲						[211]
	▲							▲			[212]
	▲		▲			▲					[213]
2013	▲								▲		[214]
	▲		▲			▲					[215]
	▲		▲		▲			▲			[216]
		▲									[217]
		▲			▲		▲				[52]
				▲							[218]
			▲		▲						[219]
2014	▲			▲							[220]
	▲		▲		▲						[221]
	▲			▲							[216]
	▲				▲			▲			[222]
	▲			▲			▲		▲		[154]
		▲									[94]
	▲				▲		▲		▲		[223]
		▲		▲		▲		▲			[224]
	▲			▲		▲				▲	
	▲		▲		▲						[225]
2015	▲				▲		▲		▲		[226]
	▲		▲		▲		▲		▲		[227]
		▲				▲					[228]
			▲		▲						[229]
	▲		▲				▲				[150]
	▲				▲		▲			▲	
		▲			▲				▲		[230]

Table 4 (continued)

Year	XRD	Raman	AFM	XPS	FTIR	TEM	SEM	TGA	UV–Vis	NMR	References
2016	▲				▲		▲				[126]
			▲		▲				▲		[84]
	▲				▲		▲				[231]
										▲	
		▲		▲				▲		▲	
		▲				▲				▲	
	▲				▲		▲				[232]
	▲				▲		▲		▲		[233]
						▲					[234]
2017	▲				▲		▲		▲		[41]
			▲			▲					[54]
		▲			▲						[235]
	▲				▲		▲				[66]
	▲		▲		▲				▲		[236]
		▲				▲		▲			[237]
	▲		▲		▲						[127]
	▲						▲		▲		[238]
2018	▲					▲		▲			[43]
	▲				▲				▲		[46]
	▲		▲								[114]
			▲								[239]
	▲	▲		▲	▲					▲	[240]
		▲	▲		▲	▲					[241]
	▲		▲		▲						[242]
	▲		▲		▲	▲	▲				[130]
		▲			▲		▲	▲			[80]
		▲		▲			▲		▲		[243]
2019	▲	▲	▲		▲		▲				[244]
	▲	▲	▲	▲	▲	▲					[44]
	▲	▲			▲		▲		▲	▲	[245]
							▲				[246]
	▲	▲	▲		▲		▲	▲	▲		[247]
	▲	▲	▲		▲						[248]
			▲								[249]
	▲	▲					▲	▲		▲	[250]
		▲	▲	▲	▲		▲				[251]
						▲	▲		▲		[252]
	▲	▲			▲		▲				[253]
			▲	▲		▲					[254]
	▲				▲		▲				[255]

Table 4 (continued)

Year	XRD	Raman	AFM	XPS	FTIR	TEM	SEM	TGA	UV–Vis	NMR	References
2020	▲		▲				▲				[104]
							▲			▲	[190]
				▲		▲	▲	▲			[256]
	▲				▲	▲		▲			[257]
	▲	▲	▲		▲		▲				[258]
	▲	▲	▲				▲				[259]
	▲	▲		▲			▲				[260]
		▲	▲	▲	▲	▲					[261]
			▲		▲				▲	▲	[30]
			▲			▲	▲				[98]
						▲	▲				[262]
	▲	▲		▲	▲	▲			▲		[263]
						▲	▲				[264]
	▲	▲	▲	▲	▲	▲	▲				[265]
						▲			▲		[266]
				▲	▲		▲		▲		[267]
	▲	▲	▲		▲	▲					[268]
	▲	▲			▲		▲	▲			[269]
	▲	▲	▲		▲		▲				[270]
	▲			▲	▲	▲					[271]
	▲	▲	▲		▲	▲					[122]
					▲		▲				[272]
	▲				▲		▲				[273]
	▲	▲	▲		▲	▲		▲			[274]
	▲	▲		▲	▲		▲				[275]
				▲	▲	▲	▲	▲			[151]
		▲	▲	▲	▲		▲		▲		[276]
		▲	▲	▲	▲	▲	▲		▲		[277]
	▲						▲				[278]
		▲			▲	▲			▲		[279]
	▲		▲			▲	▲				[280]
	▲	▲	▲	▲			▲				[281]

Table 4 (continued)

Year	XRD	Raman	AFM	XPS	FTIR	TEM	SEM	TGA	UV–Vis	NMR	References
2021		▲	▲		▲	▲	▲	▲			[123]
	▲	▲		▲		▲	▲				[282]
		▲	▲		▲	▲	▲			▲	[283]
	▲	▲		▲	▲	▲			▲		[284]
	▲	▲		▲	▲		▲				[285]
							▲				[286]
	▲	▲	▲		▲	▲	▲	▲			[287]
	▲	▲		▲	▲	▲	▲			▲	[288]
	▲			▲	▲		▲				[289]
	▲	▲	▲	▲	▲	▲	▲				[290]
	▲	▲	▲	▲	▲		▲	▲			[291]
	▲	▲		▲		▲	▲				[124]
		▲	▲	▲	▲	▲	▲				[292]
	▲	▲	▲		▲			▲			[293]
		▲			▲		▲		▲		[294]
					▲		▲				[295]
	▲	▲	▲		▲	▲		▲			[296]
	▲	▲			▲		▲				[297]
	▲	▲	▲				▲		▲		[298]
	▲	▲			▲		▲			▲	[299]
	▲	▲				▲	▲		▲		[300]
	▲	▲			▲	▲	▲				[301]
	▲	▲			▲		▲				[302]
	▲	▲		▲	▲	▲	▲	▲	▲		[120]
		▲		▲	▲	▲			▲		[303]
		▲			▲				▲		[304]
	▲	▲		▲	▲	▲	▲	▲			[125]
	▲	▲		▲	▲	▲	▲				[152]
	▲	▲					▲	▲			[305]
		▲	▲		▲	▲	▲				[306]
	▲	▲			▲		▲	▲			[307]
No. of studies	**97**	**103**	**61**	**57**	**92**	**72**	**86**	**37**	**34**	**23**	**150**
Utilization% (U)	**64.67**	**68.67**	**40.67**	**38.00**	**61.33**	**48.00**	**57.33**	**24.67**	**22.67**	**15.33**	
Classifications	**U ≥ 60% Primary technique (P)**			**40% ≤ U < 60% Secondary technique (S)**				**U < 40% Tertiary technique (T)**			
	P	**P**	S	T	**P**	S	S	T	T	T	-

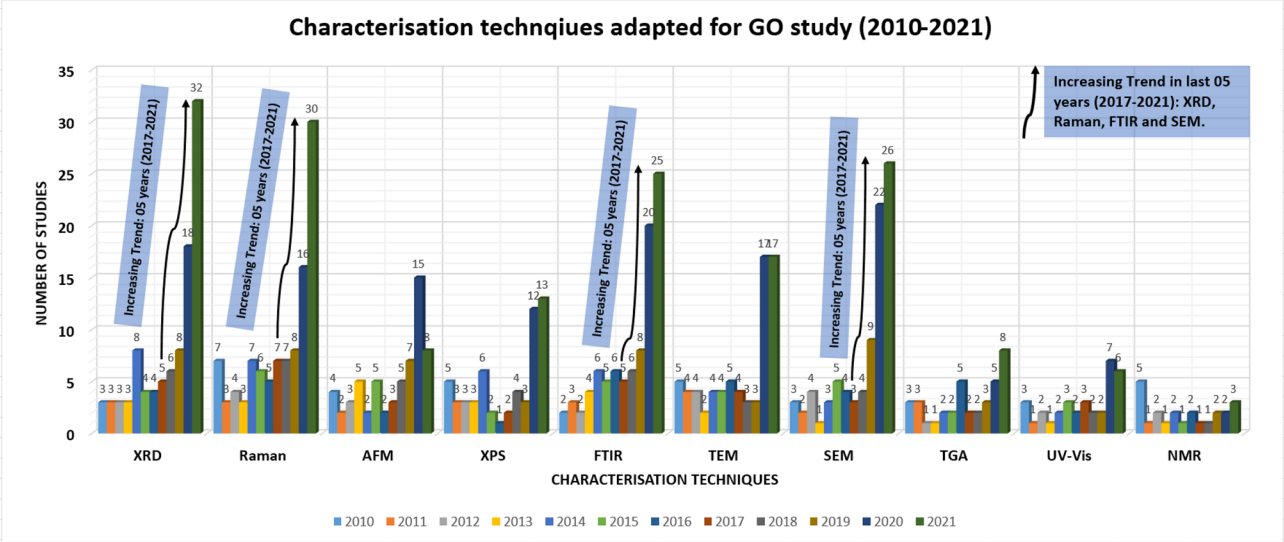

Fig. 58 Number of studies for GO characterization using different techniques from year 2010–2021

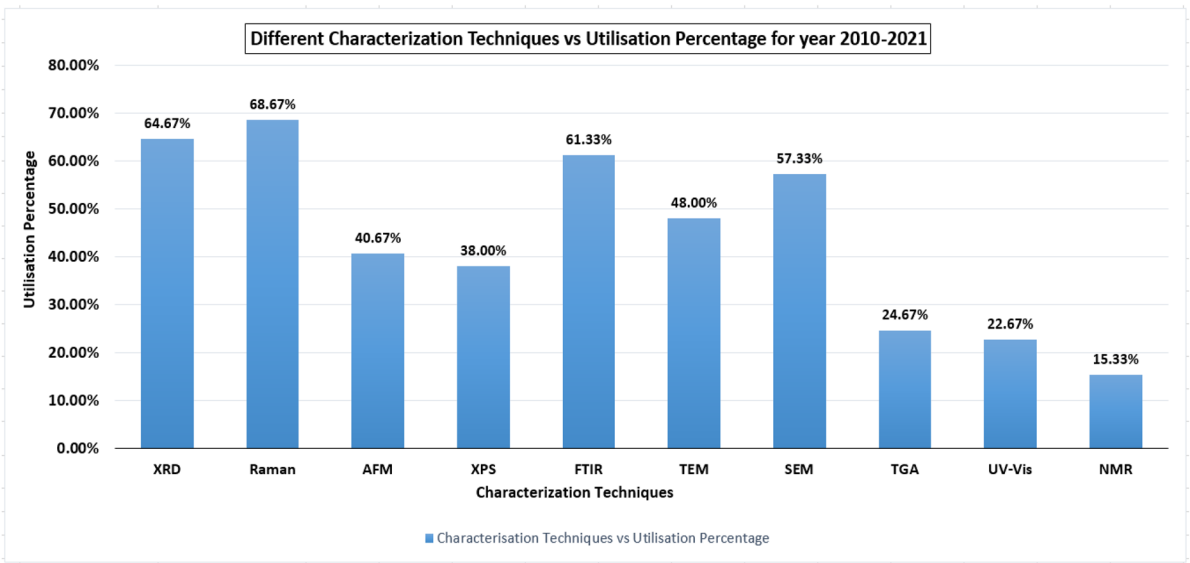

(Note: Reviewing all of the characterization literature for the last 11 years would be an impossible task. However, the objective is to illustrate the present techniques for GO characterization in contrast to their utilization weightage**)**

Fig. 59 Comparison of GO characterization techniques concerning their utilization percentage

10 Conclusion

This article provides a thorough review of the current literature regarding different synthesis methods adopted in a top-down approach for the fabrication of graphene and its derivative GO nanomaterial. Based on the literature reviewed, the chemical process is one of the most widely employed methods for the synthesis of graphene and GO. However, there are many challenges yet to come over. Synthesizing large areas and high-quality single-layer graphene oxide is still a major challenge faced by the industries. Therefore, the availability of high-quality graphene oxide for research studies is still limited; however, rapid progress is being made which may overcome this limitation shortly. Furthermore, this article also reviews the weightage of different characterization techniques adopted for the study of 2D-GO nanomaterials. According to the literature, there is no common or standard approach for GO characterization. The reason behind this is completely not clear and may be

due to instrument unavailability, author's opinion regarding the adoption of particular techniques. Figure 58 presents the number of studies carried on for GO characterization using different approaches from year 2010–2021. Figure 59 illustrates the comparative analysis of different characterization techniques based on their utilization percentage. The comparative results from 150 different literature studies were categorized into three different classifications based on their utilization proportions. Methods with utilization proportion greater than 60% are referred to as primary techniques (P), whereas greater than 40% and less than 60% are termed as secondary techniques (S). Lastly, utilization proportion less than 40% categorized as tertiary techniques (T). From Fig. 58, an incremental trend in number of studies can be observed for XRD, Raman, FTIR and SEM techniques in the last 05 years (2017–2021). It states them as the most preferred methods adopted by researchers for characterizing the GO nanomaterial. Similarly, from Fig. 59, based on the utilization scaling proportion Raman (68.67%), XRD (64.67%), and FTIR (61.33%) are the most endorsed approach for GO characterization and cited as primary techniques. Three other different techniques most frequently used includes SEM (57.33%), TEM (48%) and AFM (40.67%). Since different techniques are utilized for different characterization parameters in accordance with research objectives and disciplines. Therefore, the lesser utilization weightage of other techniques does not represents their lower effectiveness and incompetency. It only illustrates the further need for in-depth research on the relevant parameters determined by these methods and probability to explore the unrevealed potential of this wondrous GO nanomaterial. Moreover, the complex structure of GO makes it difficult to suggest a standard characterization approach as for different applications different characteristics are essential. However, the basic parameters which are most relevant to all studies include the presence of functional groups, degree of disorder or defects in its structure, the elemental composition of carbon and oxygen (C:O), stacking, and lateral dimension. FTIR and XPS represent the presence of functional groups. Raman spectroscopy indicates the defect or disorder in its structure by relating the intensity of D and G band peaks. Stacking and interlayer spacing can be easily determined using the XRD approach. Flake size measurement and elemental composition (C:O) may be acquired using the SEM technique. TGA technique is adopted to analyze the thermal stability. TEM and AFM illustrate the lateral dimension of GO nanosheets whereas UV–Vis. spectroscopy helps to determine the degree of GO dispersion in an aqueous solution.

11 Future prospects

Extensive research on synthesis process and characterization methods for graphene and its oxides are available, still it trends as a subject of broad and current interest among researchers for technological advancements in different fields of engineering, medical and material sciences [264, 308]. Currently, there is no systematic synthesis approach available for its mass production in industrial process [309]. Thus, fabricating it as an expensive material and restricting its usage for practical applications on a substantial scale. Recently, in field of civil engineering, a construction firm, Nationwide Engineering in a joint venture with the University of Manchester (Graphene Engineering Innovation Centre) has laid the world's first graphene enhanced concrete slab commercially in Amesbury Solstice Park, United Kingdom (UK) [310]. It was reported that the usage of only tiny amount of graphene enhances the concrete performance almost 30% as compared to standard concrete. However, due to its costly nature and lesser production limits its usage on a wider scale [311]. Moreover, in bulk synthesis of superior quality monolayer GO is still a major challenge faced by both industries and researchers. Therefore, there is a need to establish an industry and academia joint research collaboration to develop a graphene-manufacturing model unit (G-MMU) that may examine the challenges and limitations occurs during its production process and mitigate them through the support of comprehensive research and technological development for manufacturing of high-quality graphene on larger-scale. This approach may explore the possibilities of graphene-undiscovered potential beyond the known properties that may encompass the required transformation in bulk synthesis of graphene and its derivative GO nanomaterial within economical scale.

Acknowledgements The authors would like to acknowledge the National Taiwan University of Science and Technology (NTUST), Taiwan to facilitate this research study.

Funding The authors would like to thank the National Taiwan University of Science and Technology (NTUST) for financing the research project under Research Scholarship 2021.

Declarations

Conflict of interest The authors declare that they have no competing interest.

References

1. Anwar A, Sabih A, Aqeel AS (2016) Performance of waste coconut shell as partial replacement of natural coarse aggregate in concrete. Int J Sci Eng Res 7(8):1802–1809

2. Lzgvbdines MG (2008) Nanomaterials for practical functional uses. J Alloys Compd 449:242–245
3. Konsta-gdoutos MS, Aza CA (2014) Self sensing carbon nanotube (CNT) and nanofiber (CNF) cementitious composites for real time damage assessment in smart structures. Cem Concr Compos 53:162–169
4. Nguyen HA, Chang TP, Thymotie A (2020) Enhancement of early engineering characteristics of modified slag cement paste with alkali silicate and sulfate. Constr Build Mater 230:117013
5. Chang TP, Shih JY, Yang KM, Hsiao TC (2007) Material properties of portland cement paste with nano-montmorillonite. J Mater Sci 42(17):7478–7487
6. Ramsden J (2011) Nanotechnology: an introduction. Elsevier, William Andrew
7. Adnan N, Nordin SM, Anwar A (2020) Transition pathways for Malaysian paddy farmers to sustainable agricultural practices: an integrated exhibiting tactics to adopt Green fertilizer. Land Use Policy 90:104255
8. Nguyen HA, Chang TP, Shih JY, Chen CT (2019) Influence of low calcium fly ash on compressive strength and hydration product of low energy super sulfated cement paste. Cem Concr Compos 99:40–48
9. Chen CT, Nguyen HA, Chang TP, Yang TR, Nguyen TD (2015) Performance and microstructural examination on composition of hardened paste with no-cement SFC binder. Constr Build Mater 76:264–272
10. Shih JY, Chang TP, Hsiao TC (2006) Effect of nanosilica on characterization of Portland cement composite. Mater Sci Eng A 424(1–2):266–274
11. Ahmad S, Anwar A, Mohammed BS, Bin M, Wahab A, Ahmad SA (2019) Strength behavior of concrete by partial replacement of fine aggregate with ceramic powder. Int J Recent Technol Eng 8(2):5712–5718
12. Columbia University (2013) Even with defects, graphene is strongest material in the world. Science Daily. https://www.sciencedaily.com/releases/2013/05/130531114733.htm
13. NanoMalaysia (2014) Nanomalaysia: national graphene action plan 2020. Nano Malaysia. http://www.nanomalaysia.com.my/NanoMalaysia-Programmes/National-Graphene-Action-Plan/
14. Commission E (2018) Graphene Flagship 2019 funded by European Union. Graphene Flagship 2019 funded by European Union. http://graphene-flagship.eu/project/fundingsystem/Pages/Fundingsystems.aspx
15. Foley T, Diamante L, Waters R, Gomollón-Be F (2020) Graphene flagship—annual report 2020. The Graphene Flagship, p 41
16. Chuah S, Pan Z, Sanjayan JG, Wang CM, Duan WH (2014) Nano reinforced cement and concrete composites and new perspective from graphene oxide. Constr Build Mater 73:113–124
17. Goncalves G, Marques PAAP, Granadeiro CM, Nogueira HIS, Singh MK, Gr J (2009) Surface modification of graphene nanosheets with gold nanoparticles : the role of oxygen moieties at graphene surface on gold nucleation and growth. Chem Mater 21(20):4796–4802
18. Tiwari A, Syvaarvi M (2015) Graphene materials: fundamentals and emerging applications, first. Scrivener Publishing, LLC
19. Geim AK, Novoselov KS (2007) The rise of graphene. Nat Mater 6(3):183–191
20. Wan X, Huang Y, Chen Y (2012) Focusing on energy and optoelectronic applications: a journey for graphene and graphene oxide at large scale. Acc Chem Res 45(4):598–607
21. Novoselov KS, Geim AK, Morozov SV, Zhang Y (2004) Electric field effect in atomically thin carbon films. Science (80-) 306:666–670
22. Wei Y, Yang R (2019) Nanomechanics of graphene. Natl Sci Rev 6(2):324–348
23. Shenderova OA, Zhirnov VV, Brenner DW, Shenderova OA, Zhirnov VV, Brenner DW (2002) Carbon nanostructures. Crit Rev Solid State Mater Sci 27(3–4):227–356
24. Lehtinen O, Kurasch S, Krasheninnikov AV, Kaiser U (2013) Atomic scale study of the life cycle of a dislocation in graphene from birth to annihilation. Nat Commun 4:1–7
25. Kohlschütter V, Haenni P (1918) To the knowledge of graphitic carbon and graphitic acid. J Inorg Gen Chem 105(1):121–144
26. Bernal JD (1924) The structure of graphite. Proc R Soc Ser A Math Phys Character 106(740):749–773
27. Goyenola C, Schmidt S, Hultman L, Gueorguiev GK (2014) Carbon fluoride, CFx: structural diversity as predicted by first principles. J Phys Chem C 118(12):6514–6521
28. Gadipelli S, Guo ZX (2015) Graphene-based materials: synthesis and gas sorption, storage and separation. Prog Mater Sci 69:1–60
29. Obeng Y, Srinivasan P (2011) Graphene: Is it the future for semiconductors? An overview of the material, devices, and applications. Electrochem Soc Interface 20(1):47–52
30. Gao R, Yao Y, Wang L, Wu H (2020) Fabrication and characterization of graphene oxide modified polycarboxylic by in situ polymerization. J Appl Polym Sci 137(4):1–8
31. Madurani KA, Suprapto S, Machrita NI, Bahar SL, Illiya W, Kurniawan F (2020) Progress in graphene synthesis and its application: history, challenge and the future outlook for research and industry. ECS J Solid State Sci Technol 9(9):3013
32. Shamsaei E, de Souza FB, Yao X, Benhelal E, Akbari A, Duan W (2018) Graphene-based nanosheets for stronger and more durable concrete: a review. Constr Build Mater 183:642–660
33. Lu L, Zhao P, Lu Z (2018) A short discussion on how to effectively use graphene oxide to reinforce cementitious composites. Constr Build Mater 189:33–41
34. Li W, Li X, Chen SJ, Liu YM, Duan WH, Shah SP (2017) Effects of graphene oxide on early-age hydration and electrical resistivity of Portland cement paste. Constr Build Mater 136:506–514
35. Li G, Yuan JB, Zhang YH, Zhang N, Liew KM (2018) Microstructure and mechanical performance of graphene reinforced cementitious composites. Compos Part A Appl Sci Manuf 114:188–195
36. Anwar A, Mohammed BS, Wahab MA, Liew MS (2020) Enhanced properties of cementitious composite tailored with graphene oxide nanomaterial—a review. Dev Built Environ 1(100002):1–21
37. Rafiee MA et al (2010) Fracture and fatigue in graphene nanocomposites. Small 6(2):179–183
38. Gonclaves G, Marques PAAP, Cruz SMA, Ramalho A (2012) Nanoscale graphene oxide versus functionalized carbon nanotubes as a reinforcing agent in a PMMA/HA bone cement. Nanoscale 4:2937–2945
39. Compton OC, Nguyen ST (2010) Graphene oxide, highly reduced graphene oxide, and graphene versatile building blocks for carbon-based materials. Small 6(6):711–723
40. Hong An Wong C, Pumera M (2012) Stripping voltammetry at chemically modified graphenes. RSC Adv 2(14):6068–6072
41. Olumurewa KO, Olofinjana B, Fasakin O, Eleruja MA, Ajayi EOB (2017) Characterization of high yield graphene oxide synthesized by simplified hummers method. Graphene 06(04):85–98
42. Anwar A (2016) The influence of waste glass powder as a pozzolanic material in concrete. Int J Civ Eng Technol 7(6):131–148
43. Hack R, Correia CHG, Zanon RADS, Pezzin SH (2018) Characterization of graphene nanosheets obtained by a modified hummer's method. Rev Mater 23(1):1–11
44. Zhang Z, Schniepp HC, Adamson DH, Schniepp HC, Adamson DH (2019) Characterization of graphene oxide: variations in reported approaches. Carbon NY 1–39

45. Tan C et al (2017) Recent advances in ultrathin two-dimensional nanomaterials. Chem Rev 117(9):6225–6331
46. Kaur M, Kaur H, Kukkar D (2018) Synthesis and characterization of graphene oxide using modified Hummer's method. AIP Conf Proc 1953:1–5
47. Mistralab (2009) Structure of grapheme. Mistralab. http://www.mistralab.it/approfondimenti/Telecomunicazioni_progetto2/grafene/Structureofgraphene.html.
48. Tuček J, Błoński P, Ugolotti J, Swain AK, Enoki T, Zbořil R (2018) Emerging chemical strategies for imprinting magnetism in graphene and related 2D materials for spintronic and biomedical applications. Chem Soc Rev 47(11):3899–3990
49. Lee C, Wei X, Kysar JW, Hone J (2008) Measurement of the elastic properties and intrinsic strength of monolayer graphene. Science (80-) 321(5887):385–388
50. Stankovich S et al (2006) Graphene-based composite materials. Nature 442:282–286
51. Dixit A, Dixit D, Chandrodaya VV, Kajla A (2013) Graphene: a new era of technology. Int J Emerg Technol Adv Eng 3(3):4–7
52. Berry V (2013) Impermeability of graphene and its applications. Carbon N Y 62:1–24
53. Chen JH, Jang C, Xiao S, Ishigami M, Fuhrer MS (2008) Intrinsic and extrinsic performance limits of graphene devices on SiO 2. Nat Nanotechnol 3(4):206–209
54. Liu N et al (2017) Ultratransparent and stretchable graphene electrodes. Sci Adv 3(9):e1700159
55. Peigney A, Laurent C, Flahaut E, Bacsa RR, Rousset A (2001) Specific surface area of carbon nanotubes and bundles of carbon nanotubes. Carbon N Y 39(4):507–514
56. Balandin AA et al (2008) Superior thermal conductivity of single-layer graphene. Nano Lett 8(3):902–907
57. Sheehy DE, Schmalian J (2009) Optical transparency of graphene as determined by the fine-structure constant . Phys Rev B Condens Matter Mater Phys 80(19):2–5
58. Sanchez F, Sobolev K (2010) Nanotechnology in concrete—a review. Constr Build Mater J 24:2060–2071
59. Sobolev K, Gutiérrez MF (2005) How nanotechnology can change the concrete world. Am Ceram Soc 84(11):16–20
60. Farjadian F et al (2020) Recent developments in graphene and graphene oxide: properties, synthesis, and modifications: a review. ChemistrySelect 5(33):10200–10219
61. E. Drexler, C. Peterson, G. Pergamit, S. Brand (1991) Unbounding the Future: The Nanotechnology Revolution. New York: William Morrow; 1st edition
62. Rollings E et al (2006) Synthesis and characterization of atomically thin graphite films on a silicon carbide substrate. J Phys Chem Solids 67(9–10):2172–2177
63. Anwar A, Sabih A, Mohdshrafusain S, Aqeelhmad S (2015) Salvage of ceramic waste and marble dust for the refinement of sustainable concrete. Int J Civ Eng Technol 6(69):79–92
64. Xin G, Hwang W, Kim N, Chae H (2010) A graphene sheet exfoliated with microwave irradiation and interlinked by carbon nanotubes for high-performance transparent flexible electrodes. Nanotechnology 21:1–7
65. Kosynkin DV et al (2009) Longitudinal unzipping of carbon nanotubes to form graphene nanoribbons. Nature 458(7240):872–876
66. Sharma N et al (2017) Synthesis and characterization of graphene oxide (GO) and reduced graphene oxide (rGO) for gas sensing application. Macromol Symp 376(1):1–5
67. Bhuyan MM, Uddin MSA, Islam MN (2016) Synthesis of graphene. Int Nano Lett 6(2):65–83
68. Novoselov KS et al (2004) Electric field effect in atomically thin carbon films. Science (80-) 306(5696):666–669
69. Ci L et al (2009) Graphene shape control by multistage cutting and transfer. Adv Mater 21(44):4487–4491
70. Kamali A, Fray D (2013) Molten salt corrosion of graphite as a possible way to make carbon nanostructures. Carbon N Y 56:121–131
71. Lang B (1975) A LEED study of the deposition of carbon on platinum crystal surfaces. Surf Sci 53(1):317–329
72. Lu X, Yu M, Huang H, Ruoff RS (1999) Tailoring graphite with the goal of achieving single sheets. Nanotechnology 10(3):269–272
73. Adetayo A, Runsewe D (2019) Synthesis and fabrication of graphene and graphene oxide: a review. Open J Compos Mater 09(02):207–229
74. Pu N-W, Wang C-A, Sung Y, Liu Y-M, Ger M-D (2009) Production of few-layer graphene by supercritical CO2 exfoliation of graphite. Mater Lett 63:1987–1989
75. Berger M (2019) Understanding grapheme. Nanowork Infographic. https://www.nanowerk.com/what_is_graphene.php.
76. Jayasena B, Subbiah S (2011) A novel mechanical cleavage method for synthesizing few-layer graphenes. Nanoscale Res Lett 6(1):1–7
77. Li X et al (2009) Large-area synthesis of high-quality and uniform graphene films on copper foils. Science (80-) 324(5932):1312–1314
78. Subrahmanyam KS, Panchakarla LS, Govindaraj A, Rao CNR (2009) Simple method of preparing graphene flakes by an arc-discharge method. J Phys Chem C 113(11):4257–4259
79. Viculis LM, Mack JJ, Mayer OM, Hahn HT, Kaner RB (2005) Intercalation and exfoliation routes to graphite nanoplatelets. J Mater Chem 15(9):974–978
80. Baig Z, Mamat O, Mustapha M, Mumtaz A, Munir KS (2018) Investigation of tip sonication effects on structural quality of graphene nanoplatelets (GNPs) for superior solvent dispersion. Ultrason Sonochemistry 45(March):133–149
81. Vallés C et al (2008) Solutions of negatively charged graphene sheets and ribbons. J Am Chem Soc 130(47):15802–15804
82. Marcano DC et al (2010) Improved synthesis of graphene oxide. ACS Nano 4(8):4806–4814
83. Lv S, Ting S, Liu J, Zhou Q (2014) Use of graphene oxide nanosheets to regulate the microstructure of hardened cement paste to increase its strength and toughness. Cryst Eng Comm 16(36):8508–8516
84. Tung TT et al (2016) Graphene oxide-assisted liquid phase exfoliation of graphite into graphene for highly conductive film and electromechanical sensors. ACS Appl Mater Interfaces 8(25):16521–16532
85. Li X, Wang X, Zhang L, Lee S, Dai H (2008) Chemically derived, ultrasmooth graphene nanoribbon semiconductors. Science 319(5867):1229–1232
86. Li DAN, Gilje S, Kaner RB, Wallace GG, Mu MB (2008) Processable aqueous dispersions of graphene nanosheets. Nat Nanotechnol 3(2):101–105
87. Castro Neto AH, Guinea F, Peres NMR, Novoselov KS, Geim AK (2009) The electronic properties of grapheme. Rev Mod Phys 81(1):109–162
88. Niu P, Zhang L, Liu G, Cheng HM (2012) Graphene-like carbon nitride nanosheets for improved photocatalytic activities. Adv Funct Mater 22(22):4763–4770
89. Berger C et al (2006) Electronic confinement and coherence in patterned epitaxial graphene. Science (80-) 312(5777):1191–1196
90. Dato A, Radmilovic V, Lee Z, Phillips J, Frenklach M (2008) Substrate-free gas-phase synthesis of graphene sheets. Nano Lett 8(7):2012–2016
91. Del M, López PL, Palomino JLV, Silva MLS, Izquierdo AR (2016) Optimization of the synthesis procedures of graphene and graphite oxide. Recent Adv Graphene Res 6:1–21

92. Khalil I, Julkapli NM, Yehye WA, Basirun WJ, Bhargava SK (2016) Graphene-gold nanoparticles hybrid-synthesis, functionalization, and application in a electrochemical and surface-enhanced raman scattering biosensor. Materials 9(6):406
93. Yin PT, Shah S, Chhowalla M, Lee KB (2015) Design, synthesis, and characterization of graphene-nanoparticle hybrid materials for bioapplications. Chem Rev 115(7):2483–2531
94. Skoda M, Dudek I, Jarosz A, Szukiewicz D (2014) Graphene: One material, many possibilities—application difficulties in biological systems. J Nanomater 2014
95. Smith AT, LaChance AM, Zeng S, Liu B, Sun L (2019) Synthesis, properties, and applications of graphene oxide/reduced graphene oxide and their nanocomposites. Nano Mater Sci 1(1):31–47
96. Szabó T, Berkesi P, Forgó O, Josepovits K, Sanakis Y, Petridis D, Dékány I (2006) Evolution of surface functional groups in a series of progressively oxidized graphite oxides. Chem Mater 18(11):2740–2749
97. Talyzin AV, Hausmaninger T, You S, Szabó T (2013) The structure of graphene oxide membranes in liquid water, ethanol and water-ethanol mixtures. Nanoscale 6(1):272–281
98. Liu P, Hou J, Zhang Y, Li L, Lu X, Tang Z (2020) Two-dimensional material membranes for critical separations. Inorg Chem Front 7(13):2560–2581
99. Scholz W, Boehm HP (1969) Investigations on the structure of graphite oxide. Zeitschrift Fur Anorg Und Allg Chemie 236(369):327–340
100. Nakajima T, Matsuo Y (1994) Formation process and structure of graphite oxide. Carbon N Y 32(3):469–475
101. He H, Riedl T, Lerf A, Klinowski J (1996) Solid-state NMR studies of the structure of graphite oxide. J Phys Chem 100(51):19954–19958
102. Lerf A, He H, Forster M, Klinowski J (1998) Structure of graphite oxide revisited. J Phys Chem B 102(23):4477–4482
103. Szabó T et al (2006) Evolution of surface functional groups in a series of progressively oxidized graphite oxides. Chem Mater 18(11):2740–2749
104. Trikkaliotis DG, Mitropoulos AC, Kyzas GZ (2020) Low-cost route for top-down synthesis of over- and low-oxidized graphene oxide. Colloids Surf A Physicochem Eng Asp 600:12
105. Dreyer DR, Park S, Bielawski CW, Ruoff RS (2010) The chemistry of graphene oxide. R Soc Chem 39:228–240
106. Chen D, Feng H, Li J (2012) Graphene oxide: preparation, functionalization, and electrochemical applications. Chem Rev 112(11):6027–6053
107. Lui CH, Liu L, Mak KF, Flynn GW, Heinz TF (2009) Ultraflat graphene. Nat Lett 462(7271):339–341
108. Elias DC et al (2009) Control of graphene's properties by reversible hydrogenation: evidence for graphane. Science (80-) 323(5914):610–614
109. Gómez-Navarro C et al (2007) Electronic transport properties of individual chemically reduced graphene oxide sheets. Nano Lett 7(11):3499–3503
110. Eda G, Mattevi C, Yamaguchi H, Kim H, Chhowalla M (2009) Insulator to semimetal transition in graphene oxide. J Phys Chem C 113(35):15768–15771
111. Schniepp HC et al (2006) Functionalized single graphene sheets derived from splitting graphite oxide. J Phys Chem B 110(17):8535–8539
112. Yang H, Cui H, Tang W, Li Z, Han N, Xing F (2017) A critical review on research progress of graphene/cement based composites. Compos Part A Appl Sci Manuf 102:273–296
113. Gong MS, Cha JR, Hong SM, Lee C, Lee DH, Joo SW (2020) Roll-to-roll graphene oxide radon barrier membranes. J Hazard Mater 383:121148
114. Muzyka R, Drewniak S, Pustelny T, Chrubasik M, Gryglewicz G (2018) Characterization of graphite oxide and reduced graphene oxide obtained from different graphite precursors and oxidized by different methods using Raman spectroscopy. Materials (Basel) 11(7):15–17
115. Kang J, Chae J, Shul C, Jung W (2019) A study on the effects of the number of layers of graphene for flow-induced power generation on graphene/polyetrafluoroethylene membranes. Mater Lett 255:6–8
116. Shahhriary L, Athawale AA (2014) Graphene oxide synthesized by using modified hummers approach. Int J Renew Energy Environ Eng 02(01):58–63
117. Kariminejad B, Salami-Kalajahi M, Roghani-Mamaqani H (2015) Thermophysical behaviour of matrix-grafted graphene/poly(ethylene tetrasulphide) nanocomposites. RSC Adv 5(121):100369–100377
118. Shalaby A, Nihtianova D, Markov P, Staneva AD (2015) Structural analysis of reduced graphene oxide by transmission electron microscopy. Bulg Chem Commun 47(1):291–295
119. Roghani-Mamaqani H, Haddadi-Asl V, Khezri K, Salami-Kalajahi M (2014) Polystyrene-grafted graphene nanoplatelets with various graft densities by atom transfer radical polymerization from the edge carboxyl groups. RSC Adv 4(47):24439–24452
120. Al-Gaashani R, Zakaria Y, Lee OS, Ponraj J, Kochkodan V, Atieh MA (2021) Effects of preparation temperature on production of graphene oxide by novel chemical processing. Ceram Int 47(7):10113–10122
121. Singh V, Joung D, Zhai L, Das S, Khondaker SI, Seal S (2011) Graphene based materials: past, present and future. Prog Mater Sci 56(8):1178–1271
122. Guo S, Qiao X, Zhao T, Wang Y-S (2020) Preparation of highly dispersed graphene and its effect on the mechanical properties and microstructures of geopolymer. J Mater Civ Eng 32(11):04020327
123. Hadad C et al (2021) Graphene quantum dots: from efficient preparation to safe renal excretion. Nano Res 14(3):674–683
124. Wang Z et al (2021) Reduced graphene oxide thin layer induced lattice distortion in high crystalline mno2 nanowires for high-performance sodium- and potassium-ion batteries and capacitors. Carbon N Y 174:556–566
125. Zheng H, Cheng Y, Zhao R, Ye Y, Chen J (2021) An improved strategy to synthesize graphite oxide with controllable interlayer spacing as coatings for anticorrosion application. J Appl Polym Sci 138(6):1–9
126. Zhao L et al (2016) Investigation of the effectiveness of PC@GO on the reinforcement for cement composites. Constr Build Mater 113:470–478
127. Yang H, Monasterio M, Cui H, Han N (2017) Experimental study of the effects of graphene oxide on microstructure and properties of cement paste composite. Compos Part A Appl Sci Manuf 102:263–272
128. Erickson K, Erni R, Lee Z, Alem N, Gannett W, Zettl A (2010) Determination of the local chemical structure of graphene oxide and reduced graphene oxide. Adv Mater 22(40):4467–4472
129. Gómez-Navarro C et al (2010) Atomic structure of reduced graphene oxide. Nano Lett 10(4):1144–1148
130. Ying Y, Yang Y, Ying Y, He P, Deng H, Sun P (2018) Cross-flow-assembled ultrathin and robust graphene oxide membranes for efficient molecule separation. Nanotechnology 29:155602
131. Paci JT, Belytschko T, Schatz GC (2007) Computational studies of the structure, behavior upon heating and mechanical properties of graphite oxide. J Phys Chem C 111(49):18099–18111
132. Pantelic RS, Meyer JC, Kaiser U, Baumeister W, Plitzko JM (2010) Graphene oxide: a substrate for optimizing preparations of frozen-hydrated samples. J Struct Biol 170(1):152–156

133. Stankovich S et al (2007) Synthesis of graphene-based nanosheets via chemical reduction of exfoliated graphite oxide. Carbon N Y 45(7):1558–1565
134. Paredes JI, Villar-Rodil S, Solís-Fernández P, Martínez-Alonso A, Tascón JMD (2009) Atomic force and scanning tunneling microscopy imaging of graphene nanosheets derived from graphite oxide. Langmuir 25(10):5957–5968
135. Jung I et al (2007) Simple approach for high-contrast optical imaging and characterization of graphene-based sheets. Nano Lett 7(12):3569–3575
136. Blake P et al (2007) Making graphene visible. Appl Phys Lett 91(6):63124
137. Park JS, Reina A, Saito R, Kong J, Dresselhaus G, Dresselhaus MS (2009) G′ band Raman spectra of single, double and triple layer graphene. Carbon N Y 47(5):1303–1310
138. Kim J, Cote LJ, Kim F, Huang J (2010) Visualizing graphene based sheets by fluorescence quenching microscopy. J Am Chem Soc 132(1):260–267
139. Treossi E, Melucci M, Liscio A, Gazzano M, Samorì P, Palermo V (2009) High-contrast visualization of graphene oxide on dye-sensitized glass, quartz, and silicon by fluorescence quenching. J Am Chem Soc 131:15576–15577
140. Babak F, Abolfazl H, Alimorad R, Parviz G (2014) Preparation and mechanical properties of graphene oxide: cement nanocomposites. Sci World J 2014:1–11
141. Jeong H-K et al (2008) Evidence of graphitic AB stacking order of graphite oxides. J Am Chem Soc 130(3):1362–1366
142. Tong T, Fan Z, Liu Q, Wang S, Yu Q (2016) Investigation of the effects of graphene on the micro- and macro-properties of cementitious materials. Constr Build Mater 106:102–114
143. Lv S, Qiu C, Ma Y, Zhou Q (2013) Regulation of GO on cement hydration crystals and its toughening effect. Mag Concr Res 65(20):1246–1254
144. Lv S, Ma Y, Qiu C, Sun T, Liu J, Zhou Q (2013) Effect of graphene oxide nanosheets of microstructure and mechanical properties of cement composites. Constr Build Mater 49:121–127
145. Sobolkina A et al (2012) Dispersion of carbon nanotubes and its influence on the mechanical properties of the cement matrix. Cem Concr Compos 34(10):1104–1113
146. Ferrari AC (2007) Raman spectroscopy of graphene and graphite: disorder, electron-phonon coupling, doping and nonadiabatic effects. Solid State Commun 143(1–2):47–57
147. Ferrari AC et al (2006) Raman spectrum of graphene and graphene layers. Phys Rev Lett 97(18):1–4
148. Horszczaruk E, Mijowska E, Kalenczuk RJ, Aleksandrzak M, Mijowska S (2015) Nanocomposite of cement/graphene oxide—impact on hydration kinetics and Young's modulus. Constr Build Mater 78:234–242
149. Anwar A, Mohammed BS, Mubarak Bin Abdul Wahab KM, Liew MS (2021) Structural quality of graphene oxide nanosheets on the basis of defect ratio: a raman study. In: Lecture notes in mechanical engineering, 2021st ed., Kuala Lumpur, pp. 423–439
150. Beams R, Gustavo Cançado L, Novotny L (2015) Raman characterization of defects and dopants in graphene. J Phys Condens Matter 27(8):083002
151. Wang N et al (2020) Improved interfacial bonding strength and reliability of functionalized graphene oxide for cement reinforcement applications. Chem A Eur J 26(29):6561–6568
152. Zhang X, Su Y, Lei L, Wu S, Shen J (2021) Preparation of a three-dimensional modified graphene oxide via RAFT polymerization for reinforcing cement composites. Colloids Surf A Physicochem Eng Asp 610:125925
153. You Y, Ni Z, Yu T, Shen Z (2008) Edge chirality determination of graphene by Raman spectroscopy. Appl Phys Lett 93(16):163112
154. Johra FT, Lee JW, Jung WG (2014) Facile and safe graphene preparation on solution based platform. J Ind Eng Chem 20(5):2883–2887
155. Tuinstra F, Koenig JL (1970) Raman spectrum of graphite. J Chem Phys 53(3):1126–1130
156. Schönfelder R et al (2007) Purification-induced sidewall functionalization of magnetically pure single-walled carbon nanotubes. Nanotechnology 18(37)
157. Moon IK, Lee J, Ruoff RS, Lee H (2010) Reduced graphene oxide by chemical graphitization. Nat Commun 1(6)
158. Wang H, Robinson JT, Li X, Dai H (2009) Solvothermal reduction of chemically exfoliated graphene sheets. J Am Chem Soc 131(29):9910–9911
159. Zhan Y, Yang J, Meng F, Guo H, Liu X, Yang X (2012) Cross-linkable nitrile functionalized graphene oxide/poly(arylene ether nitrile) nanocomposite films with high mechanical strength and thermal stability. J Mater Chem 22(12):5602
160. Gedler G, Antunes M, Realinho V, Velasco JI (2012) Thermal stability of polycarbonate-graphene nanocomposite foams. Polym Degrad Stab 97(8):1297–1304
161. Jeong HK, Lee YP, Jin MH, Kim ES, Bae JJ, Lee YH (2009) Thermal stability of graphite oxide. Chem Phys Lett 470(4–6):255–258
162. Jeong HK et al (2008) Evidence of graphitic AB stacking order of graphite oxides. J Am Chem Soc 130(4):1362–1366
163. Hedayatian M, Vahedi K, Nezamabadi A, Momeni A (2020) Microstructural and mechanical behavior of Al6061-graphene oxide nanocomposites. Met Mater Int 26(6):760–772
164. Acik M, Lee G, Chabal YJ, Mattevi C, Chhowalla M, Cho K (2010) Unusual infrared-absorption mechanism in thermally reduced graphene oxide. Nat Mater 9(10):840–845
165. A Romani (2015) Graphene oxide as a cement reinforcing additive. Politecnico di Milano
166. Sun Y, Wang X, Song W, Lu S, Chen C, Wang X (2017) Mechanistic insights into the decontamination of Th(iv) on graphene oxide-based composites by EXAFS and modeling techniques. Environ Sci Nano 4(1):222–232
167. Kuzenkova AS et al (2019) New insights into the mechanism of graphene oxide and radionuclide interaction. Carbon N Y 158:291–302
168. Yadav AK et al (2021) Local structural investigations of graphitic ZnO and reduced graphene oxide composite. Appl Surf Sci 565:150548
169. D'Angelo D et al (2015) Electron energy-loss spectra of graphene oxide for the determination of oxygen functionalities. Carbon N Y 93:1034–1041
170. Pei S, Cheng HM (2012) The reduction of graphene oxide. Carbon N Y 50(9):3210–3228
171. Ramakrishnan MC, Thangavelu RR (2015) Synthesis and characterization of reduced graphene oxide. University of Waterloo, Ontario
172. Toh SY, Loh KS, Kamarudin SK, Daud WRW (2014) Graphene production via electrochemical reduction of graphene oxide: Synthesis and characterisation. Chem Eng J 251:422–434
173. Zhou M et al (2009) Controlled synthesis of large-area and patterned electrochemically reduced graphene oxide films. Chem A Eur J 15(25):6116–6120
174. Zeng F et al (2011) In situ one-step electrochemical preparation of graphene oxide nanosheet-modified electrodes for biosensors. Chemsuschem 4(11):1587–1591
175. Yang D et al (2009) Chemical analysis of graphene oxide films after heat and chemical treatments by X-ray photoelectron and Micro-Raman spectroscopy. Carbon N Y 47(1):145–152
176. Biniak S, Szymański G, Siedlewski J, Światkoski A (1997) The characterization of activated carbons with oxygen and nitrogen surface groups. Carbon N Y 35(12):1799–1810

177. Xu Y, Sheng K, Li C, Shi G (2011) Highly conductive chemically converted graphene prepared from mildly oxidized graphene oxide. J Mater Chem 21(20):7376–7380
178. Shao Y, Wang J, Engelhard M, Wang C, Lin Y (2010) Facile and controllable electrochemical reduction of graphene oxide and its applications. J Mater Chem 20(4):743–748
179. Paredes JI, Martı A, Tasco JMD (2008) Graphene oxide dispersions in organic solvents. Langmuir 24(19):10560–10564
180. Lu Z, Yao J, Leung CKY (2019) Using graphene oxide to strengthen the bond between PE fiber and matrix to improve the strain hardening behavior of SHCC. Cem Concr Res 126:105899
181. Xu L, Cheng L (2013) Graphite oxide under high pressure: a Raman spectroscopic study. J Nanomater 2013:1–6
182. Park S et al (2009) Colloidal suspensions of highly reduced graphene oxide in a wide variety of organic solvents. Nano Lett 9(4):1593–1597
183. De Souza FAL, Ambrozio AR, Souza ES, Cipriano DF, Scopel WL, Freitas JCC (2016) NMR spectral parameters in graphene, graphite, and related materials: Ab initio calculations and experimental results. J Phys Chem C 120(48):27707–27716
184. Vacchi IA, Spinato C, Raya J, Bianco A, Ménard-Moyon C (2016) Chemical reactivity of graphene oxide towards amines elucidated by solid-state NMR. Nanoscale 8(28):13714–13721
185. Chatham JC, Blackband SJ (2001) Nuclear magnetic resonance spectroscopy and imaging in animal research. ILAR J 42(3):189–208
186. Guo C (2017) Nuclear magnetic resonance (NMR) spectroscopic characterization of nanomaterials and biopolymers. Arizona State University
187. Bryce DL (2017) NMR crystallography: structure and properties of materials from solid-state nuclear magnetic resonance observables. IUCrJ 4(4):350–359
188. Raja PMV, Barron AR (1934) Physical methods in chemistry
189. PMV Raja, AR Barron (1934) Characterization of graphene by NMR mechanism. In Physical methods in chemistry 6–10
190. Mazur AS, Vovk MA, Tolstoy PM (2020) Solid-state 13C NMR of carbon nanostructures (milled graphite, graphene, carbon nanotubes, nanodiamonds, fullerenes) in 2000–2019: a mini-review. Fuller Nanotube Carbon Nanostruct 28(3):202–213
191. Casabianca LB et al (2010) NMR-based structural modeling of graphite oxide using multidimensional 13C solid-state NMR and ab initio chemical shift calculations. J Am Chem Soc 132(16):5672–5676
192. Mermoux M, Chabre Y, Rousseau A (1991) FTIR and 13C NMR study of graphite oxide. Carbon N Y 29(3):469–474
193. Cai W et al (2008) Synthesis and solid-state NMR structural characterization of 13C-labeled graphite oxide. Science (80-) 321:1815–1818
194. Ishii Y (2001) 13C-13C dipolar recoupling under very fast magic angle spinning in solid-state nuclear magnetic resonance: applications to distance measurements, spectral assignments, and high-throughput secondary-structure determination. J Chem Phys 114(19):8473–8483
195. Emwas AHM (2015) The strengths and weaknesses of NMR spectroscopy and mass spectrometry with particular focus on metabolomics research 1277
196. Klinowski J, Lerf A, He H, Forster M (1998) A new structural model for graphite oxide. Chem Phys Lett 287(1–2):53–56
197. Si Y, Samulski ET (2008) Synthesis of water soluble graphene. Nano Lett 8(6):1679–1682
198. Titelman GI, Gelman V, Bron S, Khalfin RL, Cohen Y, Bianco-Peled H (2005) Characteristics and microstructure of aqueous colloidal dispersions of graphite oxide. Carbon N Y 43(3):641–649
199. Hontoria-Lucas C, López-Peinado AJ, de López-González J, Rojas-Cervantes ML, Martín-Aranda RM (1995) Study of oxygen-containing groups in a series of graphite oxides: physical and chemical characterization. Carbon N Y 33(11):1585–1592
200. Luo J et al (2010) Graphene oxide nanocolloids. J Am Chem Soc 132(50):17667–17669
201. Kim J, Cote LJ, Kim F, Yuan W, Shull KR, Huang J (2010) Graphene oxide sheets at interfaces. J Am Chem Soc 132(23):8180–8186
202. Tian L et al (2010) Graphene oxides for homogeneous dispersion of carbon nanotubes. ACS Appl Mater Interfaces 2(11):3217–3222
203. Qiu L et al (2010) Dispersing carbon nanotubes with graphene oxide in water and synergistic effects between graphene derivatives. Chem A Eur J 16(35):10653–10658
204. Fan Z et al (2010) A three-dimensional carbon nanotube/graphene sandwich and its application as electrode in supercapacitors. Adv Mater 22(33):3723–3728
205. Lu X et al (2011) A flexible graphene/multiwalled carbon nanotube film as a high performance electrode material for supercapacitors. Electrochim Acta 56(14):5115–5121
206. Li Y, Wang H, Xie L, Liang Y, Hong G, Dai H (2011) MoS2 nanoparticles grown on graphene: an advanced catalyst for the hydrogen evolution reaction. J Am Chem Soc 133(19):7296–7299
207. Zhang B, Binheng Q, Huang ZD, Oh SW, Kim JK (2011) SnO2–graphene–carbon nanotube mixture for anode material with improved rate capacities. Carbon N Y 49(13):4524–4534
208. Ganguly A, Sharma S, Papakonstantinou P, Hamilton J (2011) Probing the thermal deoxygenation of graphene oxide using high-resolution in situ X-ray-based spectroscopies. J Phys Chem C 115(34):17009–17019
209. Yang S-Y et al (2011) Design and tailoring of a hierarchical graphene-carbon nanotube architecture for supercapacitors. J Mater Chem 21(7):2374–2380
210. Liu Y-Z, Chen C-M, Li Y-F, Li X-M, Kong Q-Q, Wang M-Z (2014) Crumpled reduced graphene oxide by flame-induced reduction of graphite oxide for supercapacitive energy storage. J Mater Chem A 2(16):5730–5737
211. Shao J-J et al (2012) Hybridization of graphene oxide and carbon nanotubes at the liquid/air interface. Chem Commun 48(31):3706–3708
212. Chen S, Yeoh W, Liu Q, Wang G (2012) Chemical-free synthesis of graphene-carbon nanotube hybrid materials for reversible lithium storage in lithium-ion batteries. Carbon N Y 50:4557–4565
213. Huang Z-D et al (2012) Self-assembled reduced graphene oxide/carbon nanotube thin films as electrodes for supercapacitors. J Mater Chem 22(8):3591–3599
214. Guo P, Chen P, Liu M (2013) One-dimensional porphyrin nanoassemblies assisted via graphene oxide: sheetlike functional surfactant and enhanced photocatalytic behaviors. ACS Appl Mater Interfaces 5(11):5336–5345
215. He Y et al (2013) Factors that affect pickering emulsions stabilized by graphene Oxide. ACS Appl Mater Interfaces 5(11):4843–4855
216. Yin G, Zheng Z, Wang H, Du Q, Zhang H (2013) Preparation of graphene oxide coated polystyrene microspheres by Pickering emulsion polymerization. J Colloid Interface Sci 394:192–198
217. Kim SD, Zhang WL, Choi HJ (2014) Pickering emulsion-fabricated polystyrene–graphene oxide microspheres and their electrorheology. J Mater Chem C 2(36):7541–7546
218. Che Man SH, Mohd Yusof NY, Whittaker MR, Thickett SC, Zetterlund PB (2013) Influence of monomer type on miniemulsion polymerization systems stabilized by graphene oxide as sole surfactant. J Polym Sci Part A Polym Chem 51(23):5153–5162
219. Che Man SH, Thickett SC, Whittaker MR, Zetterlund PB (2013) Synthesis of polystyrene nanoparticles 'armoured' with

nanodimensional graphene oxide sheets by miniemulsion polymerization. J Polym Sci Part A Polym Chem 51(1):47–58
220. Zhang Y, Zhang N, Tang Z-R, Xu Y-J (2014) Graphene oxide as a surfactant and support for in-situ synthesis of Au–Pd nanoalloys with improved visible light photocatalytic activity. J Phys Chem C 118(10):5299–5308
221. Tang C et al (2014) Conductive polymer nanocomposites with hierarchical multi-scale structures via self-assembly of carbon-nanotubes on graphene on polymer-microspheres. Nanoscale 6(14):7877–7888
222. Kim M, Kim DY, Kang Y, Park OO (2015) Facile fabrication of highly flexible graphene paper for high-performance flexible lithium ion battery anode. RSC Adv 5(5):3299–3305
223. Pan X, Yang M-Q, Xu Y-J (2014) Morphology control, defect engineering and photoactivity tuning of ZnO crystals by graphene oxide—a unique 2D macromolecular surfactant. Phys Chem Chem Phys 16(12):5589–5599
224. Li J, Zeng X, Ren T, van der Heide E (2014) The preparation of graphene oxide and its derivatives and their application in bio-tribological systems. Lubricants 2:137–161
225. Zhang H, Yang D, Ji Y, Ma X, Xu J, Que D (2004) Low temperature synthesis of flowerlike ZnO nanostructures by cetyltrimethylammonium bromide-assisted hydrothermal process. J Phys Chem B 108(13):3955–3958
226. Kazi SN et al (2015) Investigation on the use of graphene oxide as novel surfactant to stabilize weakly charged graphene nanoplatelets. Nanoscale Res Lett 10(1):212
227. Peng J, Weng J (2015) One-pot solution-phase preparation of a MoS2/graphene oxide hybrid. Carbon N Y 94:568–576
228. Wahid MH, Chen X, Gibson CT, Raston CL (2015) Amphiphilic graphene oxide stabilisation of hexagonal BN and MoS2 sheets. Chem Commun 51(58):11709–11712
229. Thickett SC, Zetterlund PB (2015) Graphene oxide (GO) nanosheets as oil-in-water emulsion stabilizers: influence of oil phase polarity. J Colloid Interface Sci 442:67–74
230. Liu J, Li X, Jia W, Li Z, Zhao Y, Ren S (2015) Demulsification of crude oil-in-water emulsions driven by graphene oxide nanosheets. Energy Fuels 29(7):4644–4653
231. Murugan M, Santhanam M, Sen Gupta S, Pradeep T, Shah SP (2016) Portland cement paste in comparison to popularly reviewed nanomaterials like aluminium oxide. Cem Concr Compos 70:48–59
232. Kothiyal NC, Sharma S, Mahajan S, Sethi S (2016) Characterization of reactive graphene oxide synthesized from ball - Milled graphite: Its enhanced reinforcing effects on cement nanocomposites. J Adhes Sci Technol 30(9):915–933
233. Liu Y et al (2016) Polystyrene/graphene oxide nanocomposites synthesized via pickering polymerization. Prog Org Coatings 99:23–31
234. Fang S, Chen T, Wang R, Xiong Y, Chen B, Duan M (2016) Assembly of graphene oxide at the crude oil/water interface: a new approach to efficient demulsification. Energy Fuels 30(4):3355–3364
235. Ickecan D, Zan R, Nezir S (2017) Eco-friendly synthesis and characterization of reduced graphene oxide. J Phys Conf Ser 902(1):8–12
236. Papageorgiou DG, Kinloch IA, Young RJ (2017) Mechanical properties of graphene and graphene-based nanocomposites. Prog Mater Sci 90:75–127
237. Mokhtar MM, Abo-El-Enein SA, Hassaan MY, Morsy MS, Khalil MH (2017) Mechanical performance, pore structure and micro-structural characteristics of graphene oxide nano platelets reinforced cement. Constr Build Mater 138:333–339
238. Zhou C, Li F, Hu J, Ren M, Wei J, Yu Q (2017) Enhanced mechanical properties of cement paste by hybrid graphene oxide/carbon nanotubes. Constr Build Mater 134:336–345
239. Ghazizadeh S, Duffour P, Skipper NT, Bai Y (2018) Understanding the behaviour of graphene oxide in Portland cement paste. Cem Concr Res 111(May):169–182
240. Mohammed A, Sanjayan JG, Nazari A, Al-saadi NTK (2018) The role of graphene oxide in limited long-term carbonation of cement-based matrix. Constr Build Mater 168:858–866
241. Long WJ, Fang C, Wei J, Li H (2018) Stability of GO modified by different dispersants in cement paste and its related mechanism. Materials (Basel) 11(5):1–17
242. Jiang W, Li X, Lv Y, Zhou M, Liu Z, Ren Z (2018) Cement-based materials containing graphene oxide and polyvinyl alcohol fiber : mechanical properties, durability, and microstructure. Nanomaterials 8:1–16
243. Lu Z, Ahanif A, Sun G, Liang R, Pavithraarthasarathy ZL (2018) Highly dispersed graphene oxide electrodeposited carbon fiber reinforced cement- based materials with enhanced mechanical properties. Cem Concr Compos 87:220–228
244. Korucu H, Şimşek B, Uygunoğlu T, Güvenç AB, Yartaşı A (2019) Statistical approach to carbon based materials reinforced cementitious composites: mechanical, thermal, electrical and sulfuric acid resistance properties. Compos Part B Eng 171(August):347–360
245. Kang X, Zhu X, Qian J, Liu J, Huang Y (2019) Effect of graphene oxide (GO) on hydration of tricalcium silicate (C 3 S). Constr Build Mater 203:514–524
246. Liu J, Li Q, Ph D, Xu S, Ph D, Asce M (2019) Reinforcing mechanism of graphene and graphene oxide sheets on cement-based materials. J Mater Civ Eng 31(4):1–9
247. Li G, Zhang LW (2019) Microstructure and phase transformation of graphene-cement composites under high temperature. Compos Part B Eng 166:86–94
248. Peng H, Ge Y, Cai CS, Zhang Y, Liu Z (2019) Mechanical properties and microstructure of graphene oxide cement-based composites. Constr Build Mater 194:102–109
249. Wang Q, Li S, Pan S, Cui X, Corr DJ, Shah SP (2019) Effect of graphene oxide on the hydration and microstructure of fly ash-cement system. Constr Build Mater 198:106–119
250. Xu G, Du S, He J, Shi X (2019) The role of admixed graphene oxide in a cement hydration system. Carbon N Y 148:141–150
251. Birenboim M et al (2019) Reinforcement and workability aspects of graphene-oxide-reinforced cement nanocomposites. Compos Part B 161:68–76
252. Bhoria R (2019) Enhancing liquid phase exfoliation of graphene in organic solvents with additives. In Graphene and its derivatives—synthesis and applications, InTech Open, pp 1–15
253. Qureshi TS, Panesar DK (2019) Impact of graphene oxide and highly reduced graphene oxide on cement based composites. Constr Build Mater 206:71–83
254. Kang S et al (2019) Graphene oxide quantum dots derived from coal for bioimaging : facile and green approach. Sci Rep 9(4101):1–7
255. Devi SC, Khan RA (2019) Effect of graphene oxide on mechanical and durability performance of concrete. J Mater Eng Struct 276:201–214
256. Van der Schueren B et al (2020) Polyvinyl alcohol-few layer graphene composite films prepared from aqueous colloids. Investigations of mechanical, conductive and gas barrier properties. Nanomaterials 10(5):1–14
257. R. Jothiramalingam, H. A. Al-lohedan, P. Arunachalam, and Z. Issa, "Synthesis and characterization of metal chalcogenide modified graphene sandwiched manganese oxide nanofibers on nickel foam electrodes for high performance supercapacitor applications," *J. Alloys Compd.*, pp. 1–42, 2020.
258. R. Askarnia, B. Ghasemi, S. R. Fardi, H. R. Lashgari, and E. Adabifiroozjaei, "Fabrication of high strength

aluminum-graphene oxide (GO) composites using microwave sintering," *Adv. Compos. Mater.*, pp. 1–15, 2020.
259. Paton-Carrero A, Valverde JL, Garcia-Alvarez E, Lavin-Lopez MP, Romero A (2020) Influence of the oxidizing agent in the synthesis of graphite oxide. J Mater Sci 55(6):2333–2342
260. Jakhar R, Yap JE, Joshi R (2020) Microwave reduction of graphene oxide. Carbon N Y 170:277–293
261. J. Luo, L. Yang, D. Sun, Z. Gao, K. Jiao, and J. Zhang, "Graphene Oxide 'Surfactant'-Directed Tunable Concentration of Graphene Dispersion," *Small*, vol. 16, no. 45, 2020.
262. C. H. A. Tsang, H. Huang, J. Xuan, H. Wang, and D. Y. C. Leung, "Graphene materials in green energy applications: Recent development and future perspective," *Renew. Sustain. Energy Rev.*, vol. 120, 2020.
263. Y. Shen *et al.*, "Fabrication of Composite Material with Pd Nanoparticles and Graphene on Nickel Foam for Its Excellent Electrocatalytic Performance," *Electrocatalysis*, pp. 1–14, 2020.
264. Hoseini-Ghahfarokhi M et al (2020) Applications of graphene and graphene oxide in smart drug/gene delivery: is the world still flat? Int J Nanomed 15:9469–9496
265. Sharma HB, Panigrahi S, Sarmah AK, Dubey BK (2020) High stability graphene oxide aerogel supported ultrafine Fe3O4 particles with superior performance as a Li-ion battery anode. Carbon N Y 135907
266. Vallurupalli K, Meng W, Liu J, Khayat KH (2020) Effect of graphene oxide on rheology, hydration and strength development of cement paste. Constr Build Mater 265:120311
267. Du Y, Yang J, Skariahhomas B, Li L, Li H, Nazar S (2020) Hybrid graphene oxide/carbon nanotubes reinforced cement paste: an investigation on hybrid ratio. Constr Build Mater 261:119815
268. Imanian Ghazanlou S, Jalaly M, Sadeghzadeh S, Habibnejadorayem A (2020) High-performance cement containing nanosized Fe3O4—decorated graphene oxide. Constr Build Mater 260:120454
269. Chintalapudi K, Pannem RMR (2020) The effects of graphene oxide addition on hydration process, crystal shapes, and microstructural transformation of ordinary portland cement. J Build Eng 32:101551
270. Devi SC, Khan RA (2020) Effect of sulfate attack and carbonation in graphene oxide-reinforced concrete containing recycled concrete aggregate. J Mater Civ Eng 32(11):04020339
271. Zhao L et al (2020) Experimental and molecular dynamics studies on the durability of sustainable cement-based composites: Reinforced by graphene. Constr Build Mater 257:119566
272. Gong J, Lin L, Fan S (2020) Modification of cementitious composites with graphene oxide and carbon nanotubes. SN Appl Sci 2(9):1–6
273. Lu Z, Yu J, Yao J, Hou D (2020) Experimental and molecular modeling of polyethylene fiber/cement interface strengthened by graphene oxide. Cem Concr Compos 112:103676
274. Jing G et al (2020) From graphene oxide to reduced graphene oxide: Enhanced hydration and compressive strength of cement composites. Constr Build Mater 248:118699
275. Liu X et al (2020) Effects of graphene oxide on microstructure and mechanical properties of graphene oxide-geopolymer composites. Constr Build Mater 247:118544
276. Jing G et al (2020) Introducing reduced graphene oxide to enhance the thermal properties of cement composites. Cem Concr Compos 109:103559
277. Lin J, Shamsaei E, Basquiroto de Souza F, Sagoe-Crentsil K, Duan WH (2019) Dispersion of graphene oxide–silica nanohybrids in alkaline environment for improving ordinary Portland cement composites. Cem Concr Compos 106:2020
278. Indukuri CSR, Nerella R, Madduru SRC (2020) Workability, microstructure, strength properties and durability properties of graphene oxide reinforced cement paste. Aust J Civ Eng 18(1):73–81
279. Sun H, Ling L, Ren Z, Memon SA, Xing F (2020) Effect of graphene oxide/graphene hybrid on mechanical properties of cement mortar and mechanism investigation. Nanomaterials 10(1):113
280. Zheng K, Guo Z, Cui N, Li Q, Feng L (2020) Effects of graphene oxide on the hydration of tricalcium silicate. Ceram - Silikaty 64(4):460–468
281. Liu Y et al (2020) Enhancing ultra-early strength of sulphoaluminate cement-based materials by incorporating graphene oxide. Nanotechnol Rev 9(1):17–27
282. Adel M, Ahmed MA, Mohamed AA (2021) Synthesis and characterization of magnetically separable and recyclable crumbled MgFe2O4/reduced graphene oxide nanoparticles for removal of methylene blue dye from aqueous solutions. J Phys Chem Solids 149:109760
283. Rhazouani A et al (2021) Synthesis and toxicity of graphene oxide nanoparticles: a literature review of in vitro and in vivo studies. Biomed Res Int 2021:1–19
284. Spilarewicz-Stanek K, Jakimińska A, Kisielewska A, Dudek M, Piwoński I (2021) Graphene oxide photochemical transformations induced by UV irradiation during photocatalytic processes. Mater Sci Semicond Process 123:105525
285. Ge W, Ma Q, Wang W, Jia F, Song S (2021) Synthesis of three-dimensional reduced graphene oxide aerogels as electrode material for supercapacitor application. Chem Phys 543:111096
286. Indukuri CSR, Nerella R (2021) Enhanced transport properties of graphene oxide based cement composite material. J Build Eng 37:102174
287. Huo Z et al (2021) Synthesis of zinc hydroxystannate/reduced graphene oxide composites using chitosan to improve poly(vinyl chloride) performance. Carbohydr Polym 256:117575
288. Liu C, Liu Y, Dang Z, Zeng S, Li C (2021) Enhancement of heterogeneous photo-Fenton performance of core-shell structured boron-doped reduced graphene oxide wrapped magnetical Fe3O4 nanoparticles: Fe(II)/Fe(III) redox and mechanism. Appl Surf Sci 544:148886
289. Muthu M, Yang E-H, Unluer C (2021) Resistance of graphene oxide-modified cement pastes to hydrochloric acid attack. Constr Build Mater 273:121990
290. Luo J, Fan C, Zhou X (2021) Functionalized graphene oxide/carboxymethyl chitosan composite aerogels with strong compressive strength for water purification. J Appl Polym Sci 138(12):12–13
291. Kwon Y, Liu M, Castilho C, Saleeba Z, Hurt R, Külaots I (2021) Controlling pore structure and conductivity in graphene nanosheet films through partial thermal exfoliation. Carbon N Y 174:227–239
292. Wang B et al (2021) Carbon-based 0D/1D/2D assembly with desired structures and defect states as non-metal bifunctional electrocatalyst for zinc-air battery. J Colloid Interface Sci 588:184–195
293. Yang Y et al (2021) Microstructure evolution and texture tailoring of reduced graphene oxide reinforced Zn scaffold. Bioact Mater 6(5):1230–1241
294. Zeng H, Lai Y, Qu S, Yu F (2021) Effect of graphene oxide on permeability of cement materials: an experimental and theoretical perspective. J Build Eng 41:102326
295. Liu C, Huang X, Wu YY, Deng X, Zheng Z (2021) The effect of graphene oxide on the mechanical properties, impermeability and corrosion resistance of cement mortar containing mineral admixtures. Constr Build Mater 288:123059
296. Ho VD, Gholampour A, Losic D, Ozbakkaloglu T (2021) Enhancing the performance and environmental impact of alkali-activated binder-based composites containing graphene oxide and industrial by-products. Constr Build Mater 284:122811

297. Kaur R, Kothiyal NC, Arora H (2020) Studies on combined effect of superplasticizer modified graphene oxide and carbon nanotubes on the physico-mechanical strength and electrical resistivity of fly ash blended cement mortar. J Build Eng 30:101304
298. Wei Z, Wang Y, Qi M, Bi J, Yang S, Yuan X (2021) The role of sucrose on enhancing properties of graphene oxide reinforced cement composites containing fly ash. Constr Build Mater 293:123507
299. Zhu X, Kang X, Deng J, Yang K (2021) A comparative study on shrinkage characteristics of graphene oxide (GO) and graphene nanoplatelets (GNPs) modified alkali-activated slag cement composites. Mater Struct 54(106):1–15
300. Prasad J, Singh AK, Tomar M, Gupta V, Singh K (2021) Hydrothermal synthesis of micro-flower like morphology aluminum-doped MoS2/rGO nanohybrids for high efficient electromagnetic wave shielding materials. Ceram Int 47(11):15648–15660
301. Owji E, Mokhtari H, Ostovari F, Darazereshki B, Shakiba N (2021) 2D materials coated on etched optical fibers as humidity sensor. Sci Rep 11(1):1–10
302. Florek P, Król M, Jeleń P, Mozgawa W (2021) Carbon fiber reinforced polymer composites doped with graphene oxide in light of spectroscopic studies. Materials (Basel) 14(8):1835
303. Qin W, Guodong Q, Dafu Z, Yue W, Haiyu Z (2021) Influence of the molecular structure of a polycarboxylate superplasticiser on the dispersion of graphene oxide in cement pore solutions and cement-based composites. Constr Build Mater 272:121969
304. Qi X, Zhang S, Wang T, Guo S, Ren R (2021) Effect of high-dispersible graphene on the strength and durability of cement mortars. Materials (Basel) 14(4):1–17
305. Muthu M, Ukrainczyk N, Koenders E (2021) Effect of graphene oxide dosage on the deterioration properties of cement pastes exposed to an intense nitric acid environment. Constr Build Mater 269:121272
306. Fan D, Yang S, Saafi M (2021) Molecular dynamics simulation of mechanical properties of intercalated GO/C-S-H nanocomposites. Comput Mater Sci 186:110012
307. Koçanalı A, KApaydın Varol E (2021) An experimental study on the electrical and thermal performance of reduced graphene oxide coated cotton fabric. Int J Energy Res 200:1–13
308. Ghosh D, Sarkar K, Devi P, Kim KH, Kumar P (2020) Current and future perspectives of carbon and graphene quantum dots: from synthesis to strategy for building optoelectronic and energy devices. Renew Sustain Energy Rev 135(July):2021
309. Ortega-Jimenez CH et al (2020) Current research and future perspectives on graphene synthesis. MATEC Web Conf 319:10001
310. Peleg R (2021) Graphene-based concrete used in a commercial setting for the first time. Graphene-info. https://www.graphene-info.com/graphene-based-concrete-used-commercial-setting-first-time
311. Wade A (2021) Graphene-doped concrete cuts construction emissions. Eureka 1–5